MIT Joint Program on the Science and Policy of Global Change

Constraining Climate Model Properties Using Optimal Fingerprint Detection Methods

Chris E. Forest, Myles R. Allen, Andrei P. Sokolov and Peter H. Stone

Report No. 62
May 2000

The MIT Joint Program on the Science and Policy of Global Change is an organization for research, independent policy analysis, and public education in global environmental change. It seeks to provide leadership in understanding scientific, economic, and ecological aspects of this difficult issue, and combining them into policy assessments that serve the needs of ongoing national and international discussions. To this end, the Program brings together an interdisciplinary group from two established research centers at MIT: the Center for Global Change Science (CGCS) and the Center for Energy and Environmental Policy Research (CEEPR). These two centers bridge many key areas of the needed intellectual work, and additional essential areas are covered by other MIT departments, by collaboration with the Ecosystems Center of the Marine Biology Laboratory (MBL) at Woods Hole, and by short- and long-term visitors to the Program. The Program involves sponsorship and active participation by industry, government, and non-profit organizations.

To inform processes of policy development and implementation, climate change research needs to focus on improving the prediction of those variables that are most relevant to economic, social, and environmental effects. In turn, the greenhouse gas and atmospheric aerosol assumptions underlying climate analysis need to be related to the economic, technological, and political forces that drive emissions, and to the results of international agreements and mitigation. Further, assessments of possible societal and ecosystem impacts, and analysis of mitigation strategies, need to be based on realistic evaluation of the uncertainties of climate science.

This report is one of a series intended to communicate research results and improve public understanding of climate issues, thereby contributing to informed debate about the climate issue, the uncertainties, and the economic and social implications of policy alternatives. Titles in the Report Series to date are listed on the inside back cover.

Henry D. Jacoby and Ronald G. Prinn,
Program Co-Directors

For more information, contact the Program office:

MIT Joint Program on the Science and Policy of Global Change
Postal Address: 77 Massachusetts Avenue
MIT E40-271
Cambridge, MA 02139-4307 (USA)
Location: One Amherst Street, Cambridge
Building E40, Room 271
Massachusetts Institute of Technology
Access: Telephone: (617) 253-7492
Fax: (617) 253-9845
E-mail: *globalchange@mit.edu*
Web site: *http://web.mit.edu/globalchange/*

Printed on recycled paper

Constraining Climate Model Properties Using Optimal Fingerprint Detection Methods

Chris E. Forest[1], Myles R. Allen[2,3], Andrei P. Sokolov[1] and Peter H. Stone[1]

Abstract[†]

We present a method for constraining key properties of the climate system that are important for climate prediction (climate sensitivity and rate of heat penetration into the deep ocean) by comparing a model's response to known forcings over the 20th century against climate observations for that period. We use the MIT two-dimensional (2D) climate model in conjunction with results from the UK Hadley Centre's coupled atmosphere-ocean general circulation model (AOGCM) to determine these constraints. The MIT 2D model is a zonally-averaged version of a 3D GCM which can accurately reproduce the global-mean transient response of coupled AOGCMs through appropriate choices of the climate sensitivity and the effective rate of diffusion of heat into the deep ocean. Vertical patterns of zonal mean temperature change through the troposphere and lower stratosphere also compare favorably with those generated by 3D GCMs. We compare the height-latitude pattern of temperature changes as simulated by the MIT 2D model with observed changes, using optimal fingerprint detection statistics. Interpreted in terms of a linear regression model as in Allen and Tett (1998), this approach yields an objective measure of model-observation goodness-of-fit (via the normalized residual sum of squares). The MIT model permits one to systematically vary the model's climate sensitivity (by varying the strength of the cloud feedback) and rate of mixing of heat into the deep ocean and determine how the goodness-of-fit with observations depends on these factors. This approach provides an efficient framework for interpreting detection and attribution results in physical terms. For the aerosol forcing set in the middle of the IPCC range, two sets of model parameters are rejected as being implausible when the model response is compared with observations. The first set corresponds to high climate sensitivity and low heat uptake by the deep ocean. The second set corresponds to low sensitivities for all values of heat uptake. These results demonstrate that fingerprint patterns must be carefully chosen, if their detection is to reduce the uncertainty of physically important model parameters which affect projections of climate change.

Contents

[1] Joint Program on the Science and Policy of Global Change, Massachusetts Institute of Technology, Cambridge MA 02139 USA
   Corresponding author: Chris E. Forest, Room E40-259, MIT, Cambridge MA 02139 USA (e-mail: ceforest@mit.edu)
[2] Space Science Department, Rutherford Appleton Laboratory, Chilton, Didcot, OX11 0QX, UK
[3] Department of Physics, University of Oxford, UK

1 Introduction

The projection of future climate change requires the use of complex climate models that contain uncertain representations of subgrid scale physics, and therefore differ in their depiction of climate system properties (e.g., cloud feedback, which is a major uncertainty in determing climate sensitivity, and the rate of penetration of heat into the deep ocean, which is the major determinant of how rapidly warming occurs (see Houghton et al., 1996)). Some information on properties of the climate system is contained, at least implicitly, in the results of detection and attribution studies: for example, unambiguous detection of anthropogenic greenhouse gas influence on climate is equivalent to rejecting the hypothesis of zero or negligible climate sensitivity. To date, however, the focus of such studies has been on signal detection rather than the physical implications. Consequently the identification of anthropogenic forcings as being responsible for recent climate changes has not yet led to a reduction in the large uncertainty in projections of future climate changes.

In a broad sense, two types of uncertainty exist: uncertainties associated with the representation of physical processes in the model used in the climate projections and uncertainties in the forcing scenarios of future climate. In this study, we address the former but recognize that a full assessment of uncertainty must encompass both types.

Fingerprint detection studies are conducted by running a climate model under a set of prescribed forcings and using detection diagnostics to determine whether climate change under a forced scenario can be distinguished in the climate observations from natural variability of the climate system (e.g. Hansen et al., 1997; Hasselmann, 1993, 1997; Hegerl et al., 1996, 1997; Santer et al., 1995, 1996; Tett et al., 1996). As is well known, it is difficult to estimate the true climate system variability from observations and therefore, climate models are run with equilibrium conditions for ∼1000 years to provide estimates of climate variability to be used in significance tests of climate change detection. It is unclear, however, how a positive detection

of climate change relates to an improved projection of future climate. In part, this is because the detection diagnostics are not directly linked to the properties known to be important for projections of climate change. As discussed elsewhere, the two such parameters are the equilibrium climate sensitivity to changes in radiative forcings (e.g., Houghton et al., 1996) and the rate of heat uptake by the deep ocean (Sokolov and Stone, 1998). Together, these properties describe the decadal-to-century timescale response of the climate system to a given forcing (e.g. via the global mean surface temperature).

In this paper, we show how climate change detection diagnostics can be used to quantify uncertainty in these properties and therefore quantify uncertainty in climate projections. We also examine how these uncertainties affect the attribution of recent climate changes to specific forcings. From recent results in climate change detection research, it appears that a signal of anthropogenic climate change is emerging from the noise of internal variability (Santer et al., 1996), but this signal has not yet been fully exploited for these purposes. One reason for this is that the enormous resources necessary to run three-dimensional coupled atmosphere-ocean general circulation models (AOGCM) limit the ability of researchers to adjust parameters related to the climate sensitivity or adjustment timescales. In addition, the ability to add and subtract forcings is restricted by the feasible number of simulations. By systematically exploring a model parameter space, which would be impossible to do using AOGCMs, this study provides a methodology for constraining model properties that are directly relevant to reducing uncertainty in the projection of climate change, and thus, has direct bearing on interpreting the detection and attribution results of 3D AOGCMs.

For a computationally efficient model, we use the MIT 2D statistical-dynamical climate model which was developed to examine the uncertainty in future climate projections associated with 3D climate models (Sokolov and Stone, 1998). The atmospheric model is coupled to a Q-flux diffusive ocean model that mixes temperature anomalies into the deep ocean. As discussed later, the model has explicit

adjustments to alter the climate sensitivity and the rate of heat mixing into the deep ocean. The model can be forced in the same manner as 3D AOGCMs and thus, uncertainty of the forcings can also be addressed. In particular, the magnitude of the anthropogenic aerosol forcing is highly uncertain. In addition to varying the sensitivity and the ocean diffusivity, the effective aerosol forcing can be varied and included as an uncertain parameter producing a three dimensional parameter space. In this study, however, the parametrization of the aerosol forcing remains fixed and we only examine the model response as a function of the climate sensitivity and deep-ocean heat uptake.

The model will be forced with changes in greenhouse gas, anthropogenic aerosol, and stratospheric ozone concentrations to produce a simulated climate record for the 20th century. We will produce a large number of simulations by spanning the parameter space of the two uncertain parameters and then use the optimal fingerprint detection algorithm to determine the fit between model simulation and observations. The fingerprint diagnostics provide normalized residual sum of squares statistics that can be used to assess the goodness-of-fit as a function of the uncertain model parameters. In this manner, a location in the model parameter space that best fits the observational record and a confidence region surrounding this point can be identified.

The method for quantifying these uncertainties is divided into two parts: the simulation of the 20th century climate record and the comparison of model simulations with observations using optimal fingerprint diagnostics. We first require a large sample of simulated records of climate change in which the climate model properties have been systematically varied. We use the MIT 2D statistical-dynamical climate model to provide the first. For the second, we employ a method of comparing simulations to observations that appropriately filters "noise" from the pattern of climate change. The variant of optimal fingerprinting proposed by Allen and Tett (1999) provides this tool and yields detection diagnostics that are objective estimates of model-data goodness-of-fit.

In what follows, we briefly describe the features of the MIT 2D climate model (Section 2.1) and the optimal fingerprint method (Section 2.2). We then discuss the forcings applied to simulate the 20th century climate record (Section 2.3) and the setup of the experiments (Section 2.4). In Section 3.1, we will discuss the model simulations and the physical implications for constructing fingerprint patterns. In Section 3.2, we will show the effects of filtering "noise" from the fingerprint diagnostics. This will be followed by a description of the distribution of the fingerprint statistics over the model parameter space (Section 3.3) and their impact on uncertainty in model forecasts (Section 4).

2   Models, Methods, and Experimental Setup

2.1   MIT 2D Land-Ocean Climate Model

The MIT 2D Land-Ocean Climate Model consists of a zonally averaged atmospheric model coupled to a Q-flux diffusive ocean model. The model details can be found in Sokolov and Stone (1995, 1998). The atmospheric model is a zonally averaged version of the Goddard Institute for Space Studies (GISS) Model II general circulation model (Hansen et al., 1983) with parameterizations of the eddy transports of momentum, heat, and moisture by baroclinic eddies (Stone and Yao, 1987, 1990). This version of the model has 24 latitude bands ($\Delta\phi = 7.826^o$) and 11 vertical layers with 4 layers above the tropopause. The model uses the GISS radiative transfer code in which the effects of all radiatively important trace gases, as well as aerosols, are included. The surface area of each latitude band is divided into a percentage of land, ocean, land ice, and sea ice with the surface and radiative fluxes computed separately for each surface type. This allows for appropriate treatment of radiative forcings dependent on underlying surface type such as anthropogenic aerosols. The atmospheric component of the model, therefore, simulates most of the important nonlinear dynamical interactions between components of the atmospheric system.

The climate model sensitivity, S, is defined as the equilibrium change in global-

mean surface temperature in response to a doubling of CO_2 concentrations. Although the true climate system sensitivity depends on multiple feedbacks, atmospheric GCM sensitivities vary primarily from differences in cloud feedback (Cess et al., 1990; Houghton et al., 1996). Consequently, the MIT model's sensitivity is controlled by altering the cloud feedback. As in most models, the MIT model parameterizes clouds based on the vertical profile of temperature and moisture. The computed cloud fraction is modified in the following way (after Hansen et al., 1993): $C' = (1 + k\Delta T_s)C$ where k is an adjustable parameter, ΔT_s is the change in global-mean surface temperature, and C is the computed cloud fraction. An increased cloud fraction (positive k) leads to a reduction of the overall warming associated with an increased external radiative forcing and vice versa. Because the additional cloud fraction is proportional to the change in temperature from equilibrium, the current mean climate remains unchanged when the climate sensitivity is changed. As discussed in Sokolov and Stone (1998), changes in atmospheric response to a doubling of CO_2 follow closely those shown by the UKMO GCM in simulations with different cloud parameterizations (Senior and Mitchell, 1993). The ability to vary the sensitivity of the MIT climate model, along with the computational efficiency, provides a useful tool for exploring questions which would be impractical to explore with more complex 3D AOGCMs.

The ocean component of the MIT model is a diffusive ocean in which temperature anomalies in the ocean mixed layer are mixed vertically into the deep ocean. The mixed-layer depths are specified from climatology, and vary with latitude and season. The ocean model's vertical diffusion coefficients depend on latitude and have been adjusted to match observations of vertical mixing as determined from tritium observations (for a description, see Sokolov and Stone, 1998). From the tritium measurements, the estimate of the globally averaged vertical diffusion coefficient, K_v, is 2.5 cm^2/s (Hansen et al., 1997) with unspecified uncertainty. The timescale, τ, for the response of the climate system to instantaneous forcings depends on the sensitivity, the mixed layer depth, and the vertical diffusion coefficient in the ocean

6

(Hansen et al., 1985). The value of the effective vertical diffusion coefficient is not well constrained by observations and differs considerably from one coupled GCM to another (Sokolov and Stone, 1998). Thus, the adjustment of the vertical diffusion of heat provides a parameter for changing the timescale of the climate system response independently of the sensitivity. The adjustment scales the meridional profile of the diffusivities such that the global mean diffusivity changes while the distribution with latitude remains fixed.

The ocean model includes the application of a Q-flux to account for horizontal heat transports in the ocean. Thus, an imposed meridional heat flux is applied in the ocean mixed layer. This Q-flux is calculated from an equilibrium climate simulation using present-day SST and sea-ice distributions and it varies seasonally. The Q-flux is imposed in all runs discussed herein. Thus, the ocean model is not purely diffusive but contains a fixed transport component. The imposed heat flux in conjunction with the vertical diffusion of heat represents all oceanic circulations. In addition the Q-flux implicitly compensates for any errors in the atmospheric model's physics. The Q-flux follows standard practice in the climate modeling community in that it is based on current climate conditions because the appropriate equilibrium conditions remain unknown for initializing simulations starting in the pre-industrial era. The model also contains an interactive thermodynamic sea-ice model, like that in the GISS GCM (Hansen et al., 1984).

In summary, the MIT model has two global parameters that determine the rate and magnitude of the decadal-to-century timescale response of the climate system to an external forcing. These are the climate sensitivity (S) to a doubling of CO_2 concentrations and the global mean vertical thermal diffusivity (K_v) of the deep ocean. Sokolov and Stone (1998) have shown that the global response of a given 3D AOGCM can be duplicated by the MIT 2D model with an appropriate choice of these two parameters for any forcing (Figure 1). Given these matching parameters, | Fig. 1 | we can then estimate the response of the 3D AOGCMs under identical forcings by the equivalent response of the 2D model (Figure 2). | Fig. 2 |

Published values of 3D AGCM model sensitivities range from 1.9^o to 5.2^oC (Senior and Mitchell, 1993). Comparisons between timeseries of transient climate changes calculated with the MIT model and with 3D AOGCMs show that the GCM's equivalent vertical diffusivities range from 0.0 to 25.0 cm^2/s (see Table 1). We intend to constrain these parameters by using comparisons of simulations with the MIT model with observations. Provided the model response over some range of these parameters differs significantly from the observations, we will be able to discard certain parameter choices as being unlikely based on the model-data goodness-of-fit.

$\boxed{\textbf{Table 1}}$

2.2 Optimal fingerprint detection statistics

The method for comparing the climate model data to the observational record is derived from the optimal fingerprint detection algorithm (e.g. Allen and Tett, 1999; Hasselmann, 1979, 1993, 1997; Hegerl and North, 1997). The technique requires choosing a pattern of climate change to be identified in the climate record and designing an optimal filter to maximize the signal-to-noise ratio in the corresponding pattern amplitude. The optimization procedure requires an *a priori* estimate of noise expected in the chosen fingerprint. Thus, we attempt to minimize the impact of fluctuations that are not associated with the signal we are trying to detect. In a perfect world, we would use an estimate of the noise based on observations. Because available data do not permit this, noise characteristics are estimated from an equilibrium control run of a climate model that simulates the natural fluctuations of the climate system as represented by the model.

The *a priori* noise estimate is given by the noise covariance matrix, $\hat{C}_N$, and is estimated from the control run of the HadCM2 model, which is one of the few AOGCMs for which extended control integrations are readily available (Tett et al., 1997). The internal variability of the vertical patterns of temperature change for timescales less than 20 years has been examined and shown to be similar to estimates from radiosonde observations (Gillett et al., 2000). Currently, no observations are available for testing the variability on longer timescales. Given that short timescale variabil-

8

ity contributes to that on longer timescales, $\hat{C}_N$ represents the natural variability in any predicted pattern, and is determined by the variability in the corresponding pattern amplitude in successive segments of "pseudo-observations" extracted from the control run for the climate model. The MIT 2D Climate Model underestimates the noise covariance matrix (Sokolov and Stone, 1998). Estimates of the MIT 2D model's variability given in Sokolov and Stone (1998) were obtained from 200-year simulations. Variability estimates based on 1000-year simulations are somewhat larger, but still smaller than those from AOGCMs.

Next, we present the optimal fingerprint method followed by the modifications necessary for this study. We have a vector of observations, $\mathbf{y}$, over a given period and a corresponding simulation (or ensemble) by the climate model, denoted by $\mathbf{x}$. We wish to determine the amplitude of the pattern, $\mathbf{x}$, that best explains the observations, $\mathbf{y}$. This is done using a multivariate regression algorithm:

$$\mathbf{y} = \sum_{i=1}^{m} \beta_i \mathbf{x}_i + \mathbf{u} \tag{1}$$

where β_i is the amplitude of the ith model-predicted pattern, $\mathbf{x}_i$, and $\mathbf{u}$ is the noise term and represents an additive internal climate variability as well as unmodeled components of the climate change. Here, $\mathbf{x}_i$ can represent either multiple model responses to individual forcings or the single response to multiple forcings. The pattern amplitudes, β_i, represent the amount by which we have to scale the i-th model-predicted signal to reproduce the observations, assuming no prior knowledge of the amplitude of any of these signals and taking into account the noise characteristics of the internal variability.

The pattern amplitudes, β_i, are determined from the standard multivariate regression algorithm:

$$\tilde{\beta} = (\mathbf{x}^T C_N^{-1} \mathbf{x})^{-1} \mathbf{x}^T C_N^{-1} \mathbf{y} \tag{2}$$

where $C_N = \mathcal{E}(\mathbf{u}\mathbf{u}^T)$. The $(\tilde{\cdot})$ denotes an optimal estimator as opposed to a standard least squares estimator and $\mathcal{E}$ represents the expectation operator. The uncertainties

in $\tilde{\beta}_i$ are estimated by:

$$\tilde{V}(\tilde{\beta}) = F_1^T C_{N_2} F_1 \tag{3}$$

where $F_1^T = (\mathbf{x}^T C_{N_1}^{-1} \mathbf{x})^{-1} \mathbf{x}^T C_{N_1}^{-1}$. $\hat{C}_{N_1}$ and $\hat{C}_{N_2}$ are estimated from separate portions of the control run to remove "artificial skill" in estimates of confidence intervals for $\tilde{\beta}$ as discussed in Allen and Tett (1999). The assumption that $\mathbf{u}$ is normally distributed is verified by checking that the normalized residual sum of squares is not inconsistent with a $F_{\kappa-m,\nu}$ distribution with $\kappa - m$ and ν degrees of freedom (d.f.) where κ is the number of retained EOFs in the pseudo-inverse of C_N (discussed later), m is the number of model patterns, and ν is the degrees of freedom of $\hat{C}_N$. The normalized residual sum of squares is given by:

$$r^2 = \tilde{\mathbf{u}}^T \hat{C}_N^{-1} \tilde{\mathbf{u}} \sim (\kappa - m) F_{\kappa-m,\nu} \tag{4}$$

where $F_{\kappa-m,\nu}$ is the F-distribution with $\kappa - m$ and ν d.f. A F_{ν_1,ν_2} distribution is the distribution resulting from the ratio of two χ^2 distributions with ν_1 and ν_2 d.f.; a χ^2_ν distribution results from adding the squares of ν normally distributed random variables with unit variance. In the limit of $\nu \to \infty$, $(\kappa - m) F_{\kappa-m,\nu} \to \chi^2_{\kappa-m}$. As done in the estimate of $\tilde{V}(\tilde{\beta})$, we note that the EOFs used to estimate $\tilde{u}$ and $\hat{C}_N$ are taken from different segments of the control runs to avoid "artificial skill". (Also, we have dropped the subscript on $\hat{C}_N$ to simplify the notation.)

One underlying problem of the multivariate regression procedure is the estimation of C_N^{-1}. The pseudo-inverse is used and hence, a truncation of the number of EOFs used in the expansion must be made. (Recall that the pseudo-inverse is given by $C_N^{-1} = E^T \Lambda^{-1} E$ where E is the matrix of eigenvectors of C_N (aka EOFs) and Λ is the associated diagonal matrix of eigenvalues. The truncation occurs by setting the high rank eigenvalues to zero.) Typically, this is an arbitrary task, but, by performing an F-test on the residuals, a warning flag for overfitting can be raised. In the multivariate regression algorithm, an assumption is made that the residuals cannot be distinguished from white noise. This provides a testable null hypothesis

10

regarding r^2 such that we can quantify the probability of not being inconsistent with a white-noise hypothesis. Provided we can estimate "the number of degrees of freedom for the fit" (Allen and Tett, 1999), we are able to place probability constraints on r^2 when compared against an F-distribution. We also note that r^2 is inversely related to typical goodness-of-fit statistics, such that we are searching for a minimum in r^2 to obtain a maximum in the goodness-of-fit.

The common interpretation of the truncation of EOFs is that we project the fingerprint pattern onto the dominant modes of variability which contribute to the pattern itself as determined from the external model of variability. Because C_N^{-1} becomes $E^T \Lambda^{-1} E$ we can substitute $E^T \Lambda^{-\frac{1}{2}} \Lambda^{-\frac{1}{2}} E$ for C_N^{-1} because Λ is a diagonal matrix. Thus, $\mathbf{x}^T C_N^{-1} \mathbf{x}$ is equivalent to a coordinate transformation to the eigenvector basis of C_N. In addition, each new variable has been normalized to have unit variance, which is equivalent to prewhitening the dataset. Thus, we write

$$\mathbf{x}^T C_N^{-1} \mathbf{x} = \mathbf{x}^T P^T P \mathbf{x} = (P\mathbf{x})^T P \mathbf{x} \tag{5}$$

where $P = \Lambda^{-\frac{1}{2}} E$. If we recognize that the EOFs are the modes of variability of the fingerprint pattern (and not the modes of climate variability from which the EOFs were estimated), we can interpret the optimal detection procedure as first projecting both the fingerprint pattern and the observation pattern onto the modes of variability and retaining only a strictly defined number of EOFs. After the projection is done, the regression coefficient, β, is then determined, after which the normalized residuals are checked against a white-noise hypothesis. If the r^2 statistic is found to be inconsistent with an F-distribution for $\kappa + 1$ EOFs, but not for κ, then the truncation of EOFs is taken as κ.

The scale factor, β, is calculated to provide the best fit between the observations and model data after each data set is rotated onto the first κ EOFs and normalized. In essence, $\beta \neq 1$ provides an additional parameter to modify the climate model output before the comparison to observations. If we set $\beta = 1$ and compute r^2, we will determine the true distribution of the goodness-of-fit for the model response

in the climate model's parameter space. This removes the additional adjustment of the amplitude of the model predicted pattern. For the case of climate change detection, the ability for β to vary is essential, although $\beta = 1$ implies a perfect model response. In our case, the additional degree of freedom is not desired because we wish only to examine the model response as a function of the model parameters. In all other aspects, the calculations remain fixed. The projections onto the EOFs and the truncation number are determined while allowing β to vary after which β is set equal to 1.0 and the r^2 is computed for the intercomparisons of model response for different values of model parameters (Summary shown in Figure 3).

<div style="float:right; border:1px solid black; padding:2px">**Fig. 3**</div>

Given that we can compute r^2 using the optimal detection algorithm, the goal of this work is to locate the minimum r^2 as a function of the uncertain model parameters. Once we find the minimum, we must ask how far can the model parameters deviate from the location of the minimum r^2 before the fit with observations is no longer consistent at some level of confidence. To do this, we use a property of the estimated residuals:

$$\mathcal{E}(r^2) = \mathcal{E}(\hat{\mathbf{u}}^T \hat{C}_N^{-1} \hat{\mathbf{u}}) = \mathbf{u}^T C_N^{-1} \mathbf{u} + m F_{m,\nu} \tag{6}$$

where $\mathbf{u}$ and $\hat{\mathbf{u}}$ represent the true and estimated residuals, respectively. Thus, the r^2 at an arbitrary location must differ by $m F_{m,\nu}$, for a given significance level, to be considered different from the minimum r^2 value, or:

$$\Delta r^2 \sim m F_{m,\nu} \tag{7}$$

This provides a means for rejecting regions of model parameter space as producing a simulation that is inconsistent with the observational record. (Strictly, we are rejecting model parameters (or simulations) that are significantly different from the best fit simulation (where r^2 is minimized). If the best fit simulation does not provide a significant match ($\beta \neq 0$) with the observations, then the Δr^2 test would not provide the necessary check against the observational record.)

In all results discussed herein, model simulations are compared to upper-air temperature changes for the 1961–1995 period as estimated from radiosonde data (Park-

er et al., 1997) with adjustments to southern hemispheric data as done in Tett et al. (1996). The radiosonde data are used to calculate annual mean, zonal mean temperature fields on a latitude-height grid (e.g., see Figure 6 below). Because data are unavailable for certain regions and times, a missing value mask is obtained for both space and time. The MIT model data are regridded to the observational grid, and then sampled using the observational data mask to compute the 1961-1980 and 1986-1995 period means. Thus, the initial fingerprint pattern is the latitude-height pattern of temperature change between the two period means. The fingerprint and observational data are identical to those used in Tett et al. (1996) for simplicity in comparing results. The choice of averaging periods was made to accomodate the 1958-1995 record of radiosonde data. Additionally, the averaging period excludes the years following major volcanic eruptions, 1963-4 and 1992, (see Allen and Tett, 1999) to reduce the effect on the computed averages. This particular choice of climate change diagnostic has direct bearing on the set of chosen anthropogenic forcings and the design of the model simulations that are discussed next.

2.3   Forcings

For a given set of model parameters, we ran the model forced by changes in greenhouse gas, sulfate aerosol, and ozone concentrations starting from equilibrium at 1860. The forcings are applied in the same manner as in HadCM2 runs (Tett et al., 1996) such that the radiative forcing by the combined greenhouse gases is represented as a change in an equivalent CO_2 concentration, the sulfate aerosols alter the surface albedo, and ozone changes are taken as deviations from the climatology. We use the same forcings as in the GSO experiments of the HadCM2 model except for the ozone data. We altered the ozone concentrations to match observations (Figure 4, see Hansen et al., 1997, for description) rather than use parameterized $\boxed{\textbf{Fig. 4}}$ changes as done in Tett et al. (1996). Hereafter, we refer to the combined forcing as the GSO forcing.

The equivalent CO_2 concentrations (Figure 4) were calculated from the instanta-

13

neous radiative forcing, ΔF, obtained from the HadCM2 GSO simulation. In our calculations, ΔF is converted to a temperature change, ΔT_o, using $\Delta T_o = \Delta F(\frac{1.2}{4.3})$ where a temperature change of $1.2°C$ corresponds to a radiative forcing change of 4.3 W/m^2 from a doubling of CO_2. The CO_2 concentrations are then calculated from ΔT_o using an approximation for the GISS radiation code (Hansen et al., 1988).

The anthropogenic aerosol forcing is imposed for clear sky only conditions by adjusting the surface albedo using a multiple reflecting approximation in the boundary layer containing the aerosols (Charlson et al., 1991; Mitchell et al., 1995). (A version of the MIT model with interactive chemistry (Wang et al., 1998) is available but was not used in order to gain computational efficiency.) The sulfate aerosol loadings (Figure 4) are converted to an albedo change via

$$\Delta R_s = \beta\delta(1 - R_s)^2 sec(\theta_o) \tag{8}$$

where R_s is the surface albedo, β is the upward scattering parameter, and θ_o is the solar zenith angle (notation from Mitchell et al. (1995)). The loading contribution is $\delta = \alpha B_{SO_4^{2-}}$ where α is the mass scattering coefficient [m^2/g] and $B_{SO_4^{2-}}$ is the sulfate loading burden [g/m^2] (see Mitchell et al., 1995). A key point is that the albedo change is dependent on the underlying surface albedo such that the effects over land and sea are different. Because the ocean albedo is smaller, the effect of the aerosols is potentially greater over the sea surface. The response to aerosol forcings remains uncertain such that neither α nor $B_{SO_4^{2-}}$ are well known (Houghton et al., 1996). To be consistent with the HadCM2 simulations we use $\alpha = 8.0$ m^2/g (Mitchell et al., 1995) which results in an annual mean radiative forcing of -0.5 W/m^2 in 1986. This compares with -0.6 W/m^2 for HadCM2. Also following Mitchell et al. (1995), we use the latitude-longitude distribution from Langner and Rodhe (1991) as an estimate of the aerosol loading pattern calculated for the 1986 emissions estimate. We compute zonal averages over land and sea surfaces to obtain the aerosol loading as a function of latitude and surface type. These latitude profiles are then scaled by the annual mean emissions estimate for the 1860-1995 period. Because the estimated residence

time for sulfate aerosols is on the order of weeks, the estimate based on the annual emissions should be a reasonable proxy for scaling the sulfate loading pattern.

2.4   Model experiments

The model experiments are designed to simulate the climate response to the prescribed GSO forcing with a particular choice of model parameters which are proxies for properties of the climate system. We created a four-member ensemble experiment for each parameter setting following Tett et al. (1996) to reduce noise in the predicted response to the climate forcings resulting from internal variability of the model. The model runs were started in 1860 with the prescribed forcing and run to 1995. At the beginning of 1940, the model was stopped and the model state perturbed by adding deviations from a control run to create the additional members of the ensemble. The model perturbations were created as outputs every 10 years from a present-day climate control run. The deviations are calculated with respect to the climatology of the control. In this manner, three perturbation runs were started in 1940 for a total of four runs with the given forcing and parameter settings. We recognize that four-member ensembles are perhaps small and that the model's efficiency would allow larger ensemble sizes. However, we chose to create a large ensemble of runs at different parameter choices rather than explore the use of a larger ensemble size at a given choice of model parameters.

Given the range of model parameters that correspond with 3D AOGCMs (see Table 1 and Figure 1), we chose to vary S in the range from 0.4 to 11.0 K and K_v from 0.0 to 160.0 cm^2/s (see Figure 2). We note that the range of S encompasses that of the IPCC (Houghton et al., 1996) cited in Kattenberg et al. (1996). Overall, these ranges cover a distribution that is known to encompass values for 3D coupled climate models (see Table 1) as well as showing significant variations in model response. For example, if we examine the decadal-mean global-mean surface temperature at the time of CO_2 doubling for a simulation in which the model is forced by a 1.0%/year rise in CO_2 concentration, the temperature change from equilibrium varies from 0.3

to 3.7 K over the parameter choices as shown in Figure 2.

We ran the model to obtain the model response to the GSO forcing as it varies within the 2D model parameter space. In all, we ran 61 experiments at different model parameter values and 4 ensemble members for each parameter setting, which corresponds to 18,544 years of simulated time. Having generated the model data, we calculated the fingerprint detection and the r^2 statistics.

3 Results

This section will be split into several parts with the intent to give the reader: (1) a sense that the model is able to produce results similar to 3D AOGCM experiments, (2) an interpretation of how the optimal fingerprint filters the data, and (3) an application of the method to a 35 year record of radiosonde data and model simulations.

3.1 Model Response

Given simulations of zonally averaged climate for 1860–1995, we can calculate two patterns of temperature change which are directly comparable to 3D AOGCM results. The first is the horizontally averaged vertical profile of temperature trends for the 1979–1995 period (Figure 5). The importance of the correct ozone concentrations for this period is clearly shown by the lack of a strong cooling trend in the stratosphere for runs which do not include the ozone concentration changes. The results shown are for values of K_v=2.5 cm^2/s and S=3.0 K and the relevant permutations of the combined forcings. As noted in Hansen et al. (1997) and Bengtsson et al. (1999), these model results indicate the importance of the appropriate ozone concentrations in providing an explanation of the trends in satellite derived estimates of similar trends over the 1979-1995 period. Although this 1D pattern of change is not used in fingerprint studies, it does show the necessity for a complete set of forcings when making a direct comparison with observations of upper-air temperature changes.

$\boxed{\textbf{Fig. 5}}$

16

The second pattern of temperature change is the latitude-height cross-section of zonal mean temperature differences for the 1961-1980 to 1986-1995 periods (Figure 6). For the GSO forcing scenario, Figure 6 shows the MIT model response for three cases that can be considered high-, middle-, and low-response parameter choices (see Figure 2). Qualitatively, the pattern of zonal mean temperature differences shows a warmer troposphere and a cooler stratosphere overall with regions of enhanced warming in the tropical upper troposphere and near the surface in polar regions. These features are consistent with theoretical expectations of changes due to GHG forcing plus feedbacks associated with water vapor, lapse rate adjustments, and high latitude albedo.

We now discuss the similarity between the HadCM2 simulation and the equivalent simulation by the MIT model. In Figure 7, the relative amplitudes of the EOFs are shown for the MIT and HadCM2 GSO simulations with equivalent changes in ozone concentrations. The amplitudes have a correlation of 0.60 and 0.83, for the optimized and non-optimized cases respectively. This further signifies that the MIT model is capable of reproducing 3D AOGCM results. In the non-optimized case, the amplitudes of the first EOF in each model are roughly -1.3. We also note that the effect of applying the optimization increases the relative amplitudes of the EOFs which will be discussed later.

Here, we note two features of the GSO response (Figure 6) that will be addressed later. First, the stratospheric cooling is relatively constant in the three cases shown. We would expect this because the cooling associated with ozone losses should be independent of both the climate sensitivity and the diffusive mixing of heat into the deep ocean. The total stratospheric cooling should be only slightly dependent on sensitivity because the greenhouse gas response shows only a small cooling in the upper stratosphere which is also almost independent of S and K_v. This invariant feature of the pattern has implications for designing fingerprint diagnostics that can be used to constrain model parameters. A second notable feature is the qualitative difference in the high latitude warming between either the low or middle case and the

Fig. 6

Fig. 7

17

high response case. The strong response in the southern latitudes appears when a significant fraction of sea ice melts and the reduced albedo enhances further warming. This will be important for further discussions of the feedback mechanisms.

3.2   Filtered Response

The optimal fingerprint algorithm as described earlier is equivalent to deriving an optimal filter to compare model simulations and observations. To illustrate the filtering process, we show the observational data after it is filtered by the optimized and non-optimized filters (Figure 8). (The non-optimal filter is that which projects the data onto the first κ EOFs but does not weight the EOF amplitudes by the inverse of the noise, i.e. the singular values.) The optimal filter emphasizes climate changes associated with what appears as shifts in the Hadley Circulation. The non-optimal filter emphasizes a broad region of warming over most of the earth with two main areas in the upper troposphere in northern mid-latitudes and in the tropics. The effect of weighting the EOF pattern by its associated variance gives more weight to the high rank EOFs with low variance. When we consider the patterns and variance of the high rank EOFs (Figure 9 and 10), the banded features of EOFs 11–14 dominate the optimized fingerprint pattern (Figure 8).

$\boxed{\text{Fig. 8}}$

$\boxed{\text{Fig. 9}}$

$\boxed{\text{Fig. 10}}$

As others have noted (Allen and Tett, 1999; Hegerl and North, 1997), the use of high rank EOFs is highly suspect if the climate noise data is insufficient to correctly sample these modes of variability. While we do not show the climate noise variance explained by EOFs, the cumulative variance of the observational data explained by the EOFs (Figure 10) shows that the first two EOFs explain 77% of the spatial variance in the observational data and the remaining 12 EOFs explain another 6% of the variance. Clearly, a relatively small amount of information is contained in the high rank EOFs but we still rely on the information in EOFs 3-14.

18

3.3 GSO Response - K_v fixed

We now present results for comparing the model response to GSO forcing with the radiosonde observations. In this first case, we compare the model response to GSO forcings for different climate sensitivities and hold K_v constant at 2.5 and 40.0 cm^2/s (Figure 11). Also we remind the reader that we compare the model response directly with observations without additional scaling by β (*i.e.*, $\beta = 1$). In these figures, two types of comparisons are made against the (1) observations and (2) pseudo-observations. We use pseudo-observations as given by the model response at a best fit location. (For each value of K_v, a best fit location is chosen by locating the minimum r^2 when a comparison is made against observations. In this case, the comparison of the model response with itself will yield $r^2 = 0$. Thus, the r^2-values of the "perfect model" must be inflated such that the minimum value matches that from the comparison with observations.) In Figure 11, we compare two methods for estimating confidence intervals for climate sensitivity, S. The first is based on the likelihood of r^2 being different from the minimum value owing to random chance (Eq. 7) indicated by the dashed horizontal lines (80th and 95th percentiles are shown). Provided r^2 is less than this value, the model response cannot be rejected as being different from the observations. A second method for estimating confidence intervals is to use Equation (3). Given the estimates of $\tilde{\beta}$ and $\tilde{V}(\tilde{\beta})$, we apply this scale-factor to the model's sensitivity and use the associated variance to provide an optimal estimate of the climate sensitivity, ($\tilde{S} = \tilde{\beta}S \pm \sigma_{\tilde{\beta}}S$, where S is the model's climate sensitivity). The confidence intervals from this second method are shown by a horizontal bar through the minimum r^2 and represent a 2-σ limit (95% confidence interval). In the case of a 3D model where the sensitivity is fixed, this is the only available estimate for the uncertainty in the climate sensitivity based on available statistics. As expected, r^2 at the minimum matches the value for the comparison against observations because we compare the model pattern with itself and obtain a perfect fit. [A more thorough approach would be to perturb the model response with

Fig. 11

19

noise from the control run and then perform the fit, but for illustrative purposes, this method suffices.] For $K_v = 2.5$ cm^2/s, the 80% confidence interval for S is 1.7 to 3.3 K. The 95% confidence interval is 1.2 to 3.8 K. For $K_v = 40.0$ cm^2/s, the 80% confidence interval for S has a lower bound at 1.5 K but no upper bound for the region spanned by our simulations. These estimates can be compared with the 95% confidence intervals based on $\sigma_{\tilde{\beta}}$ which are 0.6 to 3.8 K and 0.2 to 3.4 K for the $K_v =2.5$ cm^2/s and 40 cm^2/s, respectively.

Using $\tilde{V}(\tilde{\beta})$ as indicated by the horizontal bar through the minimum r^2-value in Figure 11, we find a bias in the uncertainty region towards lower sensitivities but this is partially a result of a model's over or under prediction of the observations. The comparison of uncertainty bounds also indicates that the statistics for the variance of S may not have a normal distribution which results from the transfer function from β to S not having a linear form. The direct application of $V(\tilde{\beta})$ to estimate the $V(S)$ does not appear to be valid. This point has been examined by Allen et al. (1999) via an energy balance model calculation for global mean temperature. Here, we make use of the full detection methodology to make a similar point. We also show a perfect model comparison (Figure 11) in which the observations are replaced with the model response at the minimum location for a given value of K_v. We note that when the r^2 values for the model to pseudo-observation comparison are smaller than for the model to observation comparison, this implies that the model response is more similar to the other model responses than to the observations over this range of S.

3.4   GSO Response - Two Free Parameters

We further examine the set of GSO simulations by varying K_v, in addition to S, and create distributions of r^2 and β in two dimensions for the comparison of the model response with the pseudo-observations (Figure 12) and the true observations (Figure 13). From the fit with pseudo-observations (Figure 12), the model response varies weakly over a wide region of the model parameter space.   As the model

20

parameters move into the "low" or "high response" regions the r^2 values correctly show that the model responses are significantly different as Figure 6 suggests. In the model-observation fit (Figure 13), we see a similar distribution of r^2 but multiple minima indicate that differences in the predicted response contributes to noisiness in the distribution of r^2. We expect that larger ensemble sizes would reduce this uncertainty and that the associated errors in r^2 would decrease providing a smoother distribution. The thick lines and shading represent the boundaries for the 80-th, 95-th, and 99-th percentile confidence regions and indicate that only the "high response" region can be rejected at the 1% level of significance. A second region of "low response" can be rejected at the 5% level of significance. We note that using this pattern of temperature change, only the NCAR W&M model is rejected by this method. All other 3D AOGCMs (see Table 1 and Figure 2) are within the 95% confidence region of acceptable parameters. We note that the response to future climate forcings of these remaining AOGCMs does not represent the full range of possible predictions which are consistent with the observations.

The distribution of β (Figure 13) indicates the relative magnitude of the model response as compared against observations. The contour for $\beta = 1$ indicates where the magnitude of the filtered model response matches that of the observations. This implies that variations of r^2 along this line should represent differences in the modeled pattern of change. The lack of significant differences in r^2 along the $\beta = 1$ curve suggests that differences in the model response are small for a broad region of model parameters based on this temperature change diagnostic.

4   Discussion

4.1   Implications for uncertainty estimates of future climate

The ability to estimate uncertainty in predictions of future climate is strongly dependent on being able to vary uncertain physical parameters that affect the future predictions. The results presented here indicate that the full distribution of model

21

responses for variations in S and K_v is necessary to determine the true uncertainty distribution of the parameters. This identifies a significant limitation of 3D AOGCMs in which the model structure remains fixed. Thus, in order to reduce uncertainty in either S or K_v, more flexible 3D climate models would be desirable. Unfortunately, the majority, if not all, of climate models *are* structurally fixed and their climate change properties are fixed as well. To adjust for this shortcoming, studies such as this one must be used to assess the probability distribution functions (pdf) of the response. We note that the GISS model, parent of the MIT model, did have a similar adjustment for the cloud feedback and therefore can produce simulations with different climate sensitivities (Hansen et al., 1993).

As discussed in Forest et al. (2000), these results provide uncertainty estimates by placing bounds on the joint probabilities for S and K_v which can then be used to estimate limits on future climate change when used in conjunction with estimates of forcing scenarios as given by changes in greenhouse gas concentrations or aerosol loadings. As an example of such bounds we refer back to Figure 2 and compare it with Figure 13. These results imply that a 5% chance exists that the warming under a 1%/year compounded increase in CO_2 concentrations will will lie outside 0.5 to 2.9 K. These results can be compared for this particular scenario with results from the second phase of the Coupled Model Intercomparison Project (CMIP2) (Meehl et al., 2000) in which the identical simulation is being carried out for a suite of 3D AOGCMs. These joint probability distributions provide a context for intercomparing models and also allows one to calculate uncertainty estimates for simulations by any single AOGCM.

Among many possible uses of these pdfs, we can assign a quantitive probability statement to the oft quoted uncertainty in climate sensitivity, 1.5–4.5K, (Houghton et al., 1996). As briefly discussed in Forest et al. (2000), the IPCC range corresponds to roughly an 80% confidence interval which is obtained from the pdf for S evaluated at $K_v = 5.0$ cm^2/s, the value of K_v that matches the upwelling diffusion/energy balance model used in Kattenberg et al. (1996) (Chapter 6, IPCC 1995). We note

that the pdf for S is non-Gaussian, having a longer tail for higher S, which leads to the non-uniform likelihoods for being outside this interval. There is a 13% chance that S will be above 4.5 K and a 7% chance that S will be less than 1.5 K. We also note that the upper bound on S increases rapidly as K_v is increased and thus, these estimates of uncertainty for S are less robust than those for the climate predictions where the isolines of model response are roughly parallel to the isolines of r^2. This particular example highlights the need for exploring joint probability distributions as well as identifying, through further use of observations, where the "true" climate system lies in such a parameter space. Doubling or halving the value of K_v used in this exercise will certainly alter the implications.

4.2   Dependency of temperature change pattern on S or K_v

One goal of this work is to provide quantitative probabilistic bounds on S and K_v. We also desire to identify means to further tighten these constraints. At first glance, we can either use additional datasets or improve the use of existing data. To further exploit existing data, we must focus on the patterns of climate change that are most dependent on climate sensitivity or ocean heat uptake. A simple method for identifying such features is to take the set of simulations (or subset) and estimate two patterns of temperature change, one that is invariant to changes in S or K_v and a second that varies linearly with S or K_v. We present the invariant pattern and the linearly varying pattern for model simulations with $K_v = 2.5$ and 40.0 cm^2/s (Figure 14) and with S = 1.6, 3.0 and 4.5 K (Figure 15). Comparing the invariant patterns with the full response (Figure 6), we see that certain features of the model response are not useful for constraining S. For example, temperature changes in the stratosphere are invariant with S. The linearly varying component indicates that changes in the tropical upper troposphere and at the surface near the sea-ice edges are most dependent on climate sensitivity. Thus, a fingerprint that focuses on these regions would best discriminate between models with different S. Unfortunately, this pattern in the tropical upper-troposphere is also the strongest

Fig. 14

Fig. 15

23

mode of variability in the HadCM2 control run (Figure 9) which means a much larger change must be observed to be significant. In all, this exercise demonstrates the need for a better understanding of how the fingerprint pattern depends on climate system properties in addition to its dependence on the various forcings. This type of analysis would lead to alternative choices of fingerprint patterns which are designed to reduce uncertainty in model parameters.

A separate issue is how these results affect the assumption of linear superposition of fingerprint patterns in the detection and attribution algorithm. We note that the variations of ΔT associated with variations in S or K_v can be of the same magnitude as the overall temperature changes. These variations combined with the threshhold type behavior noted earlier suggests that simple combinations of fixed patterns may be inappropriate. Therefore, perhaps we should examine more closely the assumption that one can scale patterns of climate change to predict future climate change and also determine the extent to which uncertainty in these predictions can be estimated from detection diagnostics.

4.3 Dependency of detection statistics on κ

In addition to exploring the dependency of the diagnostic on properties of the climate system, we can examine the dependency of the detection statistics on truncation number. As we have already shown in Figure 13, the distribution of $\tilde{\beta}$ follows our expectations by following a typical response surface as shown in Figure 2. The regions of high (low) response require $\tilde{\beta} < 1$ ($\tilde{\beta} > 1$) to reduce (increase) the model predicted response and match the observations. The well defined $\tilde{\beta} = 1$ isoline passing through the acceptable region of parameter space adds a consistency check for the methodology. Hence, the distribution of $\tilde{\beta}$ is consistent with our understanding of the climate change detection methodology. As part of our analysis, we varied the truncation number, κ, to explore how r^2 varied. Because the lower order EOFs represent the largest spatial scales, we wished to explore the possibility that small scale features could dominate the r^2 distribution. In fact, the r^2 distribution remains

24

robust to changes in κ (Figure 16). We also explored the distribution of $\tilde{\beta}$ in the same fashion and found two strange effects. First, the position of the $\tilde{\beta} = 1$ isoline shifts dramatically as κ varies. Second, the values of $\tilde{\beta}$ for S < 1 begin to decrease for all $\kappa < 13$. For $\kappa \geq 13$, the distribution of $\tilde{\beta}$ remains fairly robust.

This behavior has bearing on two issues of the detection problem. First, the choice of κ remains a topic of debate because the level of significance for the detection and attribution results depends on the estimate of the natural variability for each EOF as determined from the control run (HadCM2, in this case.) If a model underestimates the noise in a particular EOF, the possibility of a false detection of climate change increases. If either the observations or the model project onto this pattern, then the increased weighting (through $\hat{C}_N^{-1}$) may falsely contribute to $\tilde{\beta}$ as well as reduce the uncertainty in $\tilde{\beta}$.

The second issue is that the value of $\tilde{\beta}$ guides the climate modeling community as to whether the model under- or over-predicts the response to the applied forcing. When the diagnostic is simply global mean temperature change, this hardly matters because the one can easily view whether the model reproduces the observational record. When the complexity of the optimal filter is considered, the comparison becomes less intuitive. In fact, it appears likely that particular regions, for example, high latitudes near the surface, could be over- or under-weighted and thus inappropriately contribute to $\tilde{\beta}$.

4.4 Remaining issues

This paper was intended to discuss issues that were left unexplored in Forest et al. (2000) due to limited space. Of those not discussed previously, two issues remain that affect the discussion of the uncertainties and their implications: (1) dependency of the climate variability on the climate model properties and (2) the uncertainty in the applied radiative forcing. In Forest et al. (2000), we acknowledge that we assume independence of the noise model, C_N, and the properties of the climate system being varied (S and K_v). It is well known that variability on all timescales

is related to the feedbacks within the system and hence, a link between climate sensitivity and variability should also exist (e.g., Hall and Manabe, 1999; Held and Soden, 2000). Additionally, the ocean is known to affect long-term climate variability through various mechanisms such as ENSO, NAO, or AO. This suggests that estimates of variability based on the HadCM2 control run may not be appropriate for all values of S and K_v. Preliminary results using the MIT model indicate that interannual variability depends on the model parameters. To apply these results to the fingerprint statistics which use the HadCM2 control run, we require a complete analysis of the MIT model's modes of variability and their relation to those of HadCM2. If these prove to be reasonably similar, we will be able to scale the noise estimate from the HadCM2 model.

The second issue is the uncertainty in the radiative forcings specified for the twentieth century. In these results, we have kept the aerosol forcing fixed at -0.5 W/m^2 for the 1986 distribution of aerosols. However, the uncertainty in the aerosol forcing ranges from 0 to -2.5 W/m^2 if the possible indirect effects are included (Houghton et al., 1996). We note that the forcing, as modeled by a change in surface albedo, represents the net aerosol forcing and includes the effects of all processes that would have a radiative forcing with a spatial distribution similar to that produced by the sulfate aerosols. We have not considered the anthropogenic forcing by tropospheric ozone which may offset the cooling by sulfate aerosols. We also neglect natural forcings such as variations in solar and volcanic activity. However, as noted in Tett et al. (1996), the data averaging procedure was chosen to minimize the effect of the volcanic forcings on the climate change signal by removing data in years 1963-4 and 1992 which correspond to eruptions of Mt. Agung and Mt. Pinatubo, respectively.

5   Conclusions

We have presented a method for constraining model properties that is based on the distribution of the r^2 statistic estimated from the optimal fingerprint detection

algorithm. The constrained model properties were chosen for their relevance to key physical processes that control the climate system's response to external forcings. Using patterns of climate change estimated from the record of radiosonde observations, we can place constraints on the model properties in a rigorous fashion. Two types of constraints can be estimated. A 1D constraint can be estimated assuming the remaining uncertain parameters are known *a priori*. If this is not possible, then constraints on two or more parameters may be estimated, however, the uncertainty region necessarily increases as well. As applied in this work, if the "true" K_v for the climate system is known, then confidence intervals with associated probabilities can be placed on S. If neither S nor K_v are known *a priori*, then the confidence interval is transformed into an uncertainty region and two regions of parameter space can be rejected with a given level of significance.

These results indicate that the choice of diagnostic has important implications on which model parameters can be constrained well. The use of surface or upper air data alone does not provide sufficient information to place strong constraints. An approach using a combination of each data set may help. Alternatively, comparisons can be done individually and the uncertainty regions can be combined using Bayesian statistical techniques to produce maximum likelihood constraints. Estimates of prior distributions for S and K_v would be taken from studies such as Webster and Sokolov (2000).

As discussed earlier, the transient response of the MIT model to increased radiative forcings can match the response of 3D AOGCMs for a unique S and K_v for any forcing. Thus, quantitative bounds on S and K_v provide a means for quantitatively comparing the predictive capabilities of 3D AOGCMs under similar forcings (see Figure 2). As emphasized in Forest et al. (2000), these results only reject the NCAR W&M model as being inconsistent with the radiosonde observations for the period examined. However, these results also fail to make significant distinctions among the remaining models and therefore suggest that results from individual models should not be considered independently.

References

Allen, M. and Tett, S., Checking for model consistency in optimal fingerprinting, *Clim. Dyn.*, *15*, 419–434, 1999.

Allen, M., Stott, P., Mitchell, J., Schnur, R., and Knutson, T., Uncertainty in forecasts of anthropogenic climate change, Tech. Rep. RAL-TR-1999-084, Rutherford Appleton Laboratory, Chilton, Didcot, OX11 0QX, UK, 1999.

Bengtsson, L., Roeckner, E., and Stendel, M., Why is the global warming proceeding much slower than expected?, *J. Geophys. Res.*, *104*, 3865–3876, 1999.

Cess, R., Potter, G., Blanchet, P., Boer, G., Del Genio, A., Deque, M., Dymnikov, V., Galin, V., Gates, W., Ghan, S., Kiehl, J., Lacis, A., Le Treut, H., Li, Z.-X., Liang, X.-Z., McAvaney, B., Meleshko, V., Mitchell, J., Morcrette, J.-J., Randall, D., Rikus, L., Roekner, L., Royer, J., Schlese, U., Sheinin, D., Slingo, A., Sokolov, A., Taylor, K., Washington, W., Wetherald, R., Yagai, I., and Zhang, M.-H., Intercomparison and interpretation of climate feedback processes in 19 atmospheric general circulation models, *J. Geophys. Res.*, *95*, 16 601–16 615, 1990.

Charlson, R., Langner, J., Rodhe, H., Leovy, C., and Warren, S., Perturbation of the northern hemisphere radiative balance by backscattering from anthropogenic sulfate aerosols., *Tellus*, *43AB*, 152–163, 1991.

Forest, C., Allen, M., Stone, P., and Sokolov, A., Constraining uncertainties in climate models using climate change detection methods., *Geophys. Res. Let.*, *27*, 569–572, 2000.

Gillett, N., Allen, M., and Tett, S., Modelled and observed variability in atmospheric vertical temperature structure, *Clim. Dyn.*, *16*, 49–61, 2000.

Hall, A. and Manabe, S., The role of water vapor feedback in unperturbed climate variability and global warming, *J. Climate*, *12*, 2327–2346, 1999.

Hansen, J., Russell, G., Rind, D., Stone, P., Lacis, A., Lebedeff, S., Ruedy, R., and Travis, L., Efficient three-dimensional global models for climate studies: Models I and II, *Mon. Weath. Rev.*, *111*, 609–662, 1983.

Hansen, J., Lacis, A., Rind, D., Russell, G., Stone, P., Fung, I., Ruedy, R., and Lerner, J., Climate sensitivity: Analysis of feedback mechanisms, in *Climate Processes and Climate Sensitivity, Geophysical Monograph*, edited by J. E. Hansen and T. Takahashi, vol. 29,

pp. 130–163, American Geophysical Union, Washington, D.C., 1984.

Hansen, J., Russell, G., Lacis, A., Fung, I., Rind, D., and Stone, P., Climate response times: Dependence on climate sensitivity and ocean mixing, *Science*, *229*, 857–859, 1985.

Hansen, J., Fung, I., Lacis, A., Rind, D., Lebedeff, S., Ruedy, R., Russell, G., and Stone, P., Global climate changes as forecast by goddard institute for space studies three-dimensional model, *J. Geophys. Res.*, *93*, 9341–9364, 1988.

Hansen, J., Lacis, A., Ruedy, R., Sato, M., and Wilson, H., How sensitive is the world's climate?, *Nat. Geog. Res. Explor.*, *9*, 142–158, 1993.

Hansen, J., Sato, M., Ruedy, R., Lacis, A., Asamoah, K., Beckford, K., Borenstein, S., Brown, E., Cairns, B., Carlson, B., Curran, B., de Castro, S., Druyan, L., Etwarrow, P., Ferede, T., Fox, M., Gaffen, D., Glascoe, J., Gordon, H., Hollandsworth, S., Jiang, X., Johnson, C., Lawrence, N., Lean, J., Lerner, J., Lo, K., Logan, J., Luckett, A., McCormick, M., McPeters, R., Miller, R., Minnis, P., Ramberran, I., Russell, G., Stone, P., Tegen, I., Thomas, S., Thomason, L., Thompson, A., Wilder, J., Willson, R., and Zawodny, J., Forcings and chaos in interannual to decadal climate change, *J. Geophys. Res.*, *102*, 25 679–25 720, 1997.

Hasselmann, K., On the signal-to-noise problem in atmospheric response studies, in *Meteorology of Tropical Oceans*, edited by Shawn, pp. 251–259, Royal Meteorological Society, 1979.

Hasselmann, K., Optimal fingerprints for the detection of time dependent climate change, *J. Climate*, *6*, 1957–1971, 1993.

Hasselmann, K., On multifingerprint detection and attribution of anthropogenic climate change, *Clim. Dyn.*, *13*, 601–611, 1997.

Hegerl, G. and North, G., Statistically optimal methods for detecting anthropogenic climate change, *J. Climate*, *10*, 1125–1133, 1997.

Hegerl, G., Von Storch, H., Hasselmann, K., Santer, B., Cusbasch, U., and Jones, P., Detecting greenhouse-gas-induced climate change with an optimal fingerprint method, *J. Climate*, *9*, 2281–2306, 1996.

Hegerl, G., Hasselmann, K., Cubasch, U., Mitchell, J., Roeckner, E., Voss, R., and Waszke-witz, J., Multi-fingerprint detection and attribution analysis of greenhouse gas, green-

house gas-plus-aerosol and solar forced climate change, *Clim. Dyn.*, *13*, 613–634, 1997.

Held, I. and Soden, B., Water vapor feedback and global warming, *Annual Reviews of Energy and the Environment*, *25*, in press, 2000.

Houghton, J., Meira Filho, L., Callander, B., Harris, N., Kattenberg, A., and Maskell, K., eds., *Climate Change 1995, The Science of Climate Change*, Cambridge University Press, Cambridge, UK, 1996.

Kattenberg, A., Giorgi, F., Grassl, H., Meehl, G., Mitchell, J., Stouffer, R., Tokioka, T., Weaver, A., and Wigley, T., Climate models – projections of future climate, in *Climate Change 1995, The Science of Climate Change*, edited by J. Houghton, L. Meira Filho, B. Callander, N. Harris, A. Kattenberg, and K. Maskell, pp. 285–358, Cambridge University Press, Cambridge, 1996.

Langner, J. and Rodhe, H., A global three-dimensional model of the tropospheric sulfur cycle, *J. Atmos. Chem.*, *13*, 225–263, 1991.

Meehl, G., Boer, G., Covey, C., Latif, M., and Stouffer, R., The coupled model intercomparison project (cmip), *Bull. American Meteorological Society*, *81*, 313–321, 2000.

Mitchell, J., Davis, R., Ingram, W., and Senior, C., On surface temperature, greenhouse gases, and aerosols: Models and observations, *J. Climate*, *8*, 2364–2386, 1995.

Parker, D., Gordon, M., Cullum, D., Sexton, D., Folland, C., and Rayner, N., A new global gridded radiosonde temperature data base and recent temperature trends, *Geophys. Res. Lett.*, *24*, 1499–1502, 1997.

Santer, B., Taylor, K., Wigley, T., Johns, T., Jones, P., Karoly, D., Mitchell, J., Oort, A., Penner, J., Ramaswamy, V., Schwarzkopf, M., Stouffer, R., and Tett, S., A search for human influences on the thermal structure of the atmosphere, *Nature*, *382*, 39–45, 1996.

Santer, B. D., Taylor, K., Wigley, T., Penner, J., Jones, P., and Cubasch, U., Towards the detection and attribution of an anthropogenic effect on climate, *Clim. Dyn.*, *12*, 77–100, 1995.

Senior, C. and Mitchell, J., Carbon dioxide and climate: the impact of cloud parametrizations, *J. Clim.*, *6*, 393–418, 1993.

Sokolov, A. and Stone, P., Description and validation of the MIT version of the GISS 2-D model, Report No. 2, *MIT JPSPGC*, p. 47, 1995.

Sokolov, A. and Stone, P., A flexible climate model for use in integrated assessments, *Clim. Dyn.*, *14*, 291–303, 1998.

Stone, P. and Yao, M.-S., Development of a two-dimensional zonally averaged statistical-dynamical model. part ii: the role of eddy momentum fluxes in the general circulation and their parametrization, *J. Atmos. Sci.*, *44*, 3769–3786, 1987.

Stone, P. and Yao, M.-S., Development of a two-dimensional zonally averaged statistical-dynamical model. part iii: the parametrization of the eddy fluxes of heat and moisture, *J. Clim.*, *3*, 726–740, 1990.

Tett, S., Mitchell, J., Parker, D., and Allen, M., Human influence on the atmospheric vertical temperature structure: Detection and observations, *Science*, *274*, 1170–1173, 1996.

Tett, S., Johns, T., and Mitchell, J., Global and regional variability in a coupled AOGCM, *Climate Dynamics*, *13*, 303–323, 1997.

Wang, C., Prinn, R., and Sokolov, A., A global interactive chemistry and climate model: Formulation and testing, *J. Geophys. Res.*, *103*, 3399–3417, 1998.

Webster, M. and Sokolov, A., A methodology for quantifying uncertainty in climate projections, *Climatic Change*, *in press*, 2000.

Tables

Table 1. Model Parameters for the MIT 2D Climate Model which correspond to various coupled AOGCMs.

Model	S	K_v
GFDL	3.7	5.0
ECHAM1/LSG	2.6	25.0
NCAR W&M	4.6	0.0
HadCM2	2.5*	7.5
NCAR CSM	2.1*	7.5

* These sensitivities were obtained through personal communications with the indicated modelling groups. The others were taken from the literature.

Figures
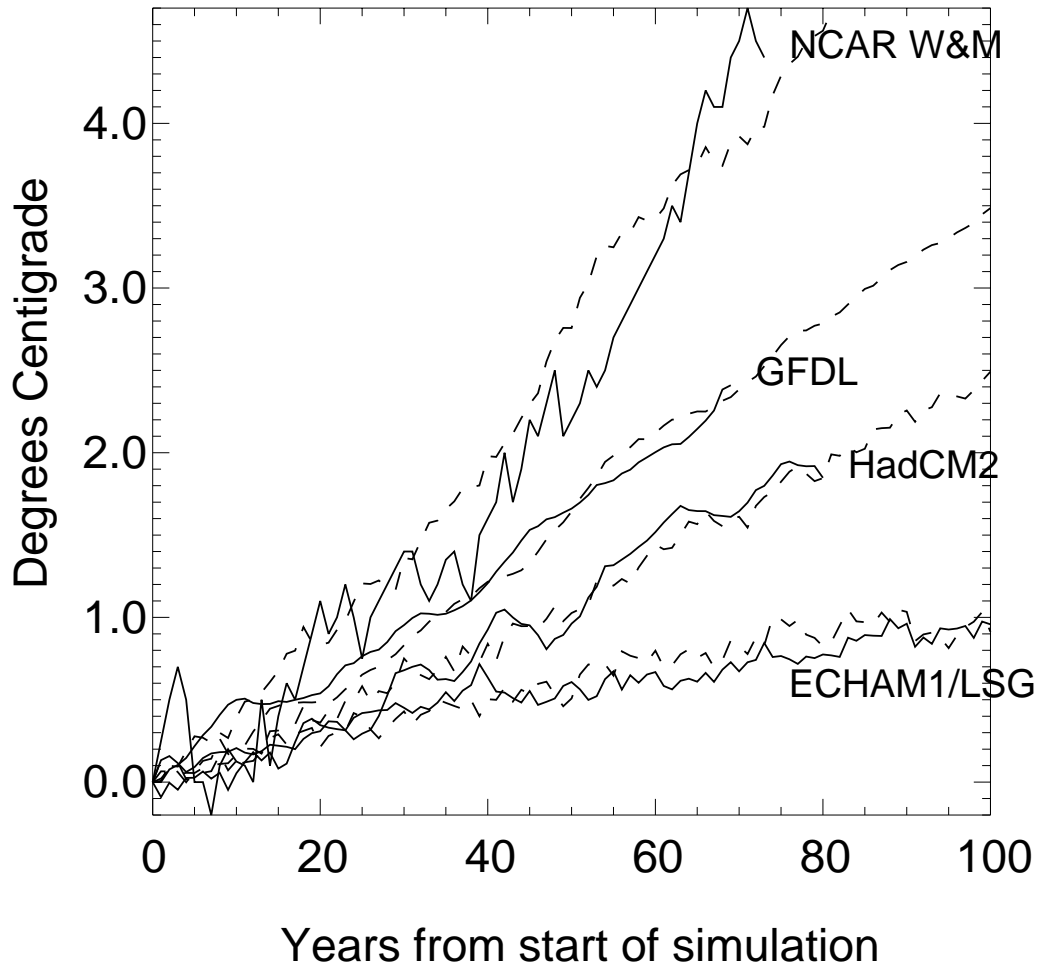
Fig. 1. Annual-mean global-mean surface temperatures for various coupled climate models (solid) and the matching MIT model (dashed) under identical forcings. The forcings were not the same in the GCM experiments.
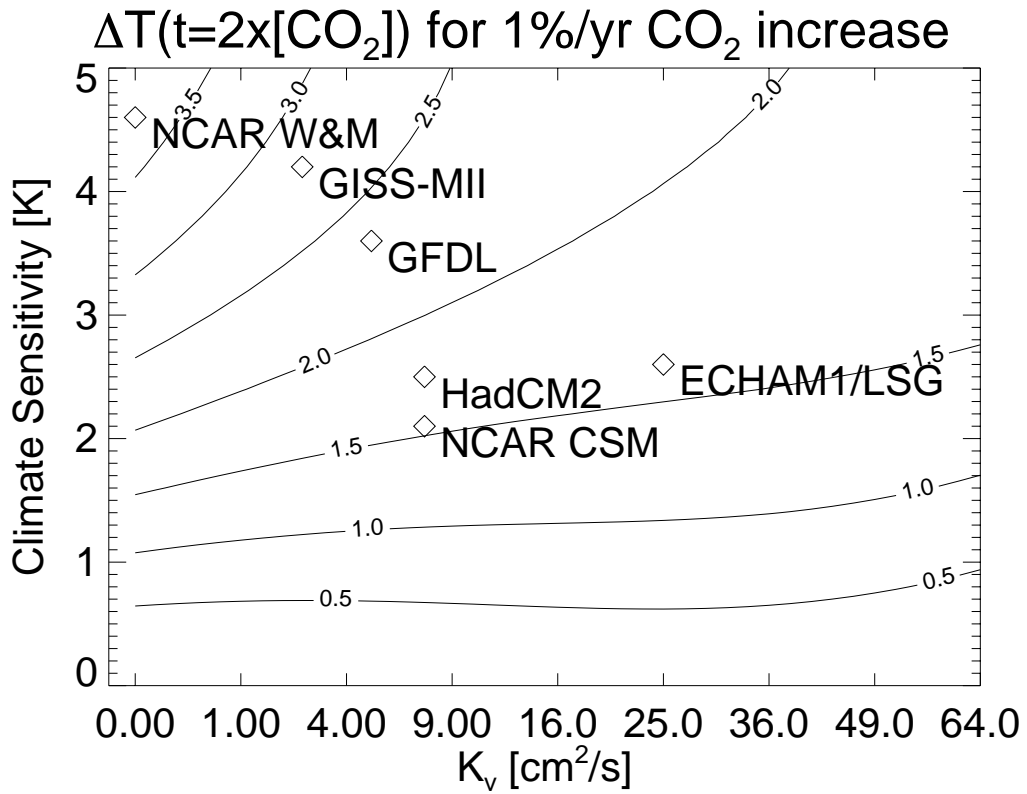
Fig. 2. Response in the global mean surface temperature at the time of doubling of CO_2 for simulations with 1%/year increase in CO_2 concentration. The corresponding S and K_v values for six AOGCMs are shown.
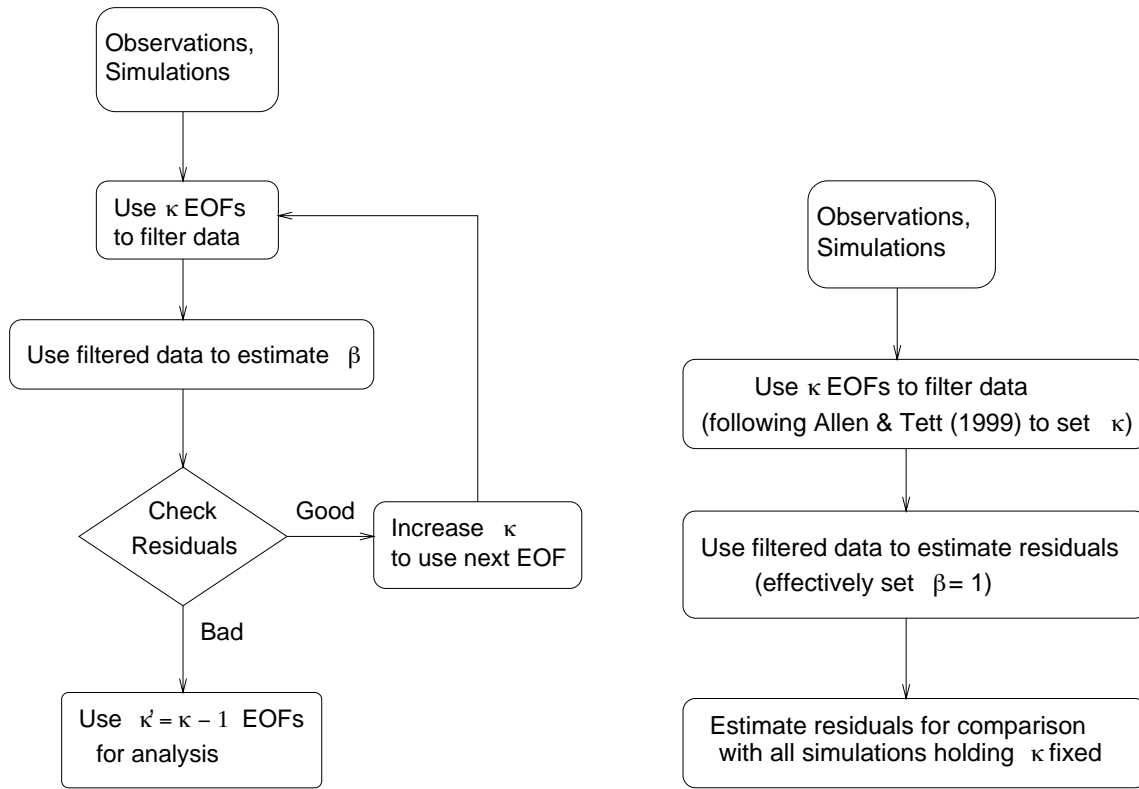
Fig. 3. Summary of optimal detection algorithm (left) and contrast with direct estimation of residuals (right).
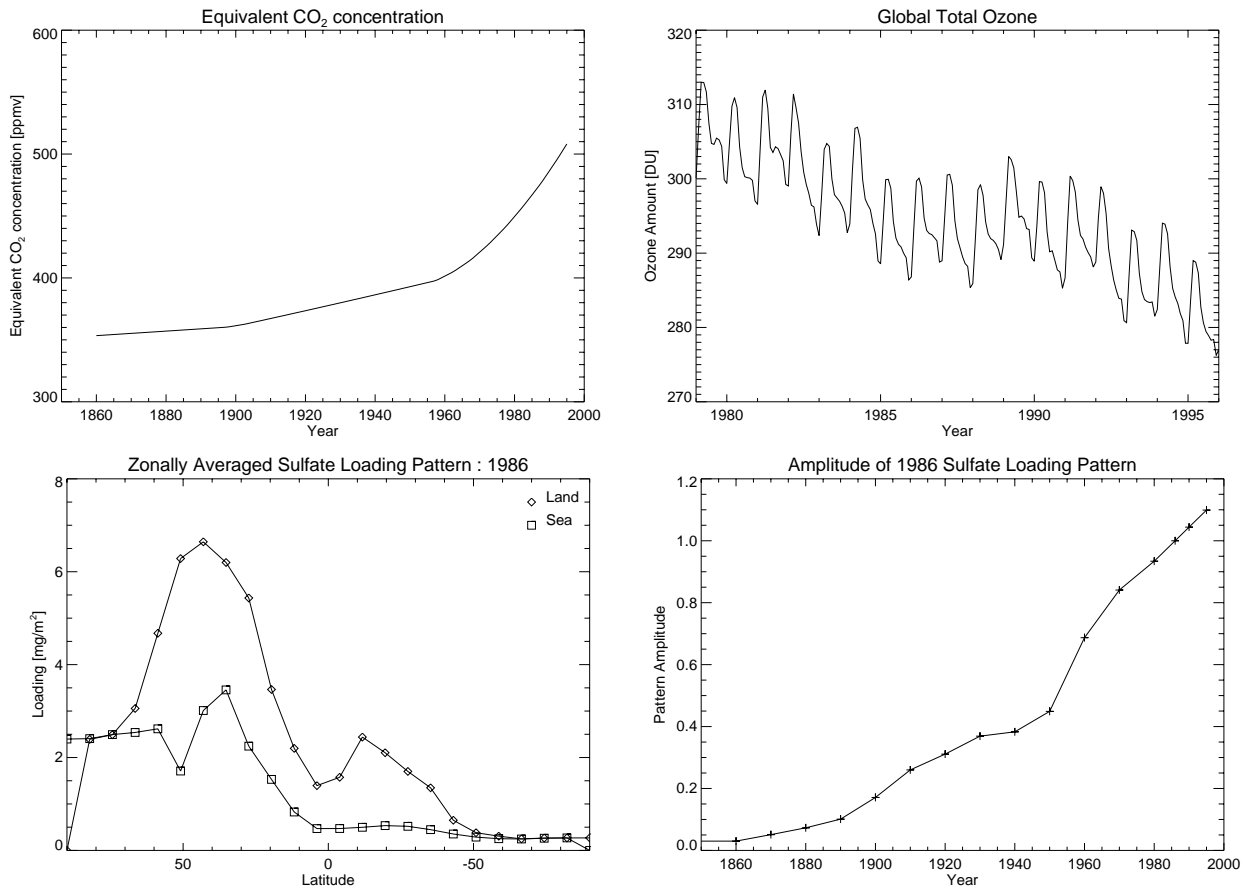
Fig. 4. Summary of applied model forcings in the MIT - GSO experiments. (A) Equivalent CO_2 is calculated from the radiative forcing diagnosed from the HadCM2 GSO experiment (see text). The ozone forcing is applied as a change in the monthly mean ozone concentration with respect to the climatological values starting in January 1979 (see text). The monthly-mean total ozone concentrations (B) illustrate the decline in concentrations from 1979–1995 (after Hansen et al. (1998)). The sulfate aerosol forcing is applied as a perturbation to the surface albedo (see text) estimated from the scaled pattern of sulfate aerosol loadings for 1986. The annual-mean zonally averaged aerosol loadings over land and ocean surfaces (C) were estimated from Langner and Rodhe (1991) and are scaled by the estimated historical sulfur emissions relative to 1986 (D), the year for which the loadings were estimated.

36
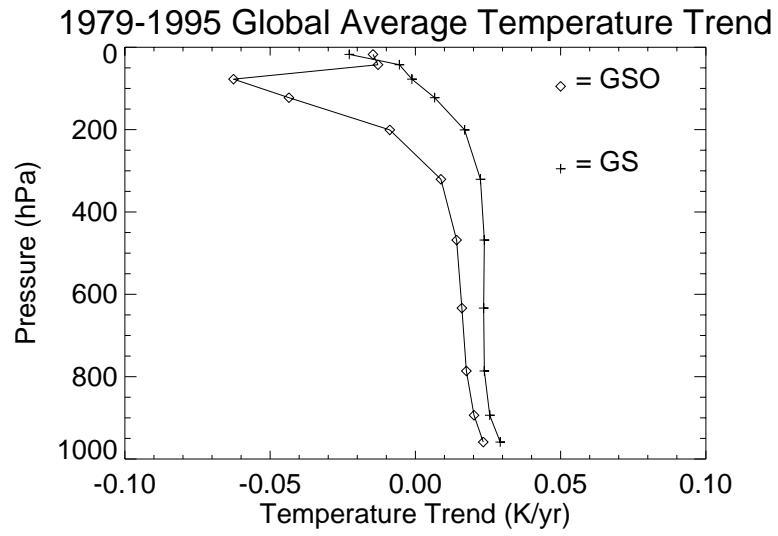
Fig. 5. The global average vertical profile for the response of the MIT model ($K_v = 2.5$ and S = 3.0) to GS and GSO forcings. The temperature trends are estimated from the 1979-1995 period.
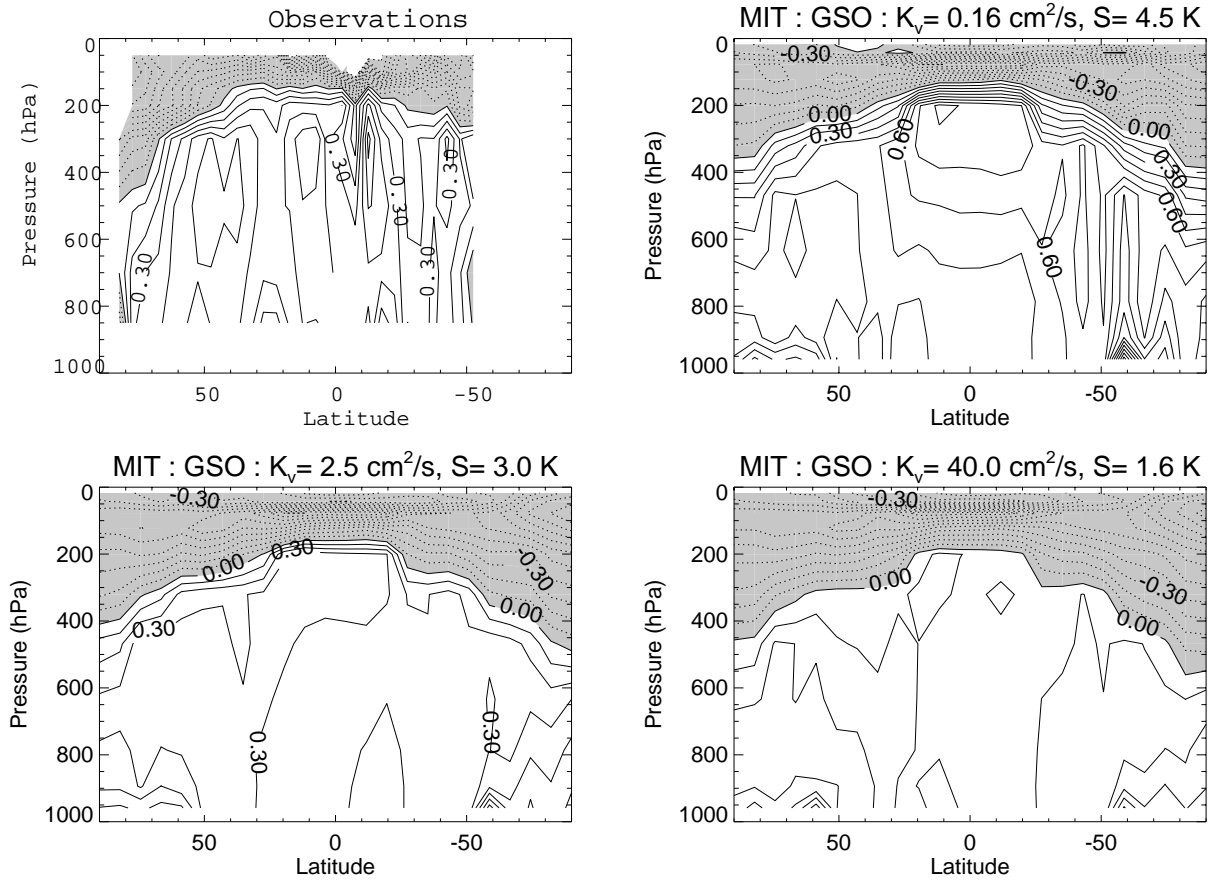
Fig. 6. Latitude-height pattern of temperature change for 1986–1995 minus 1961–1980 periods from radiosonde observations (upper left) and model simulations with $(K_v$ [cm^2/s],S [K]) = (0.16,4.5), (2.5,3.0), and (40.0,1.6) and $\alpha = 8.0$ m^2/kg. The model is forced by changes in greenhouse gas, sulfate aerosol, and ozone concentrations. The model data are shown on the model grid without the observational mask.
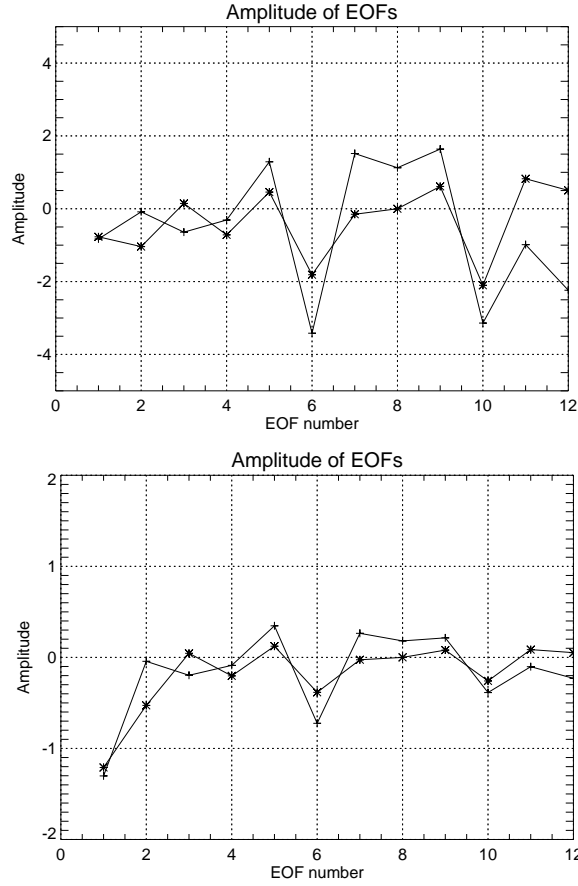
Fig. 7. Relative amplitudes of EOFs in optimized (top) and non-optimized (bottom) pattern of climate change for response of MIT model (+) with S = 2.5 K and K_v = 7.5 cm^2/s and for HadCM2-GSO ($*$) experiment. In this case only, the MIT model uses the same changes in ozone concentrations as used in the HadCM2-GSO experiment. The amplitudes are estimated by computing the EOFs of the noise covariance matrix, $\hat{C}_N$, scaling the EOFs by the square root of one over the eigenvalues, and then taking the projection of the model response onto the normalized EOFs. The optimally filtered pattern is the linear combination of the optimized EOF patterns multiplied by the respective coefficients shown here.
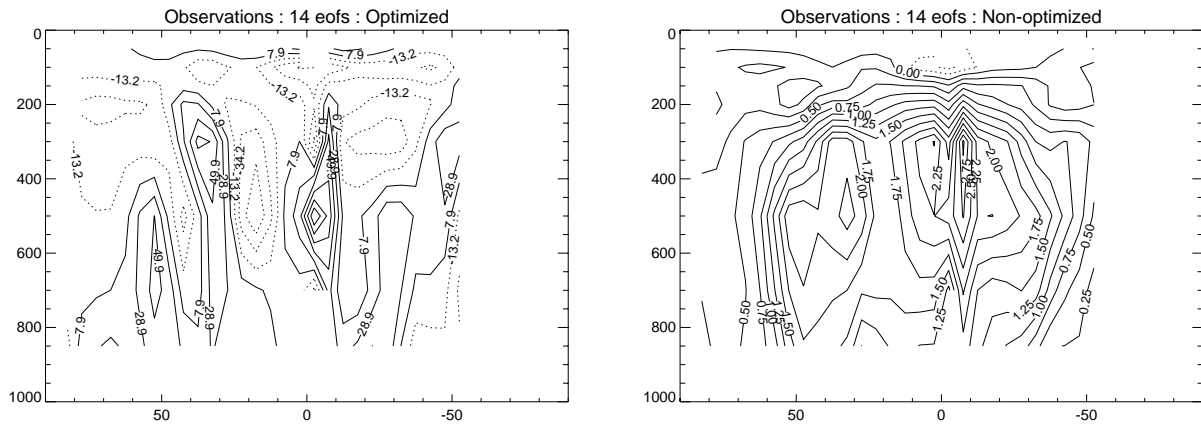
Fig. 8. Optimal and non-optimal filtered patterns of climate change as estimated from the radiosonde observations using the EOFs from the HadCM2 control run.
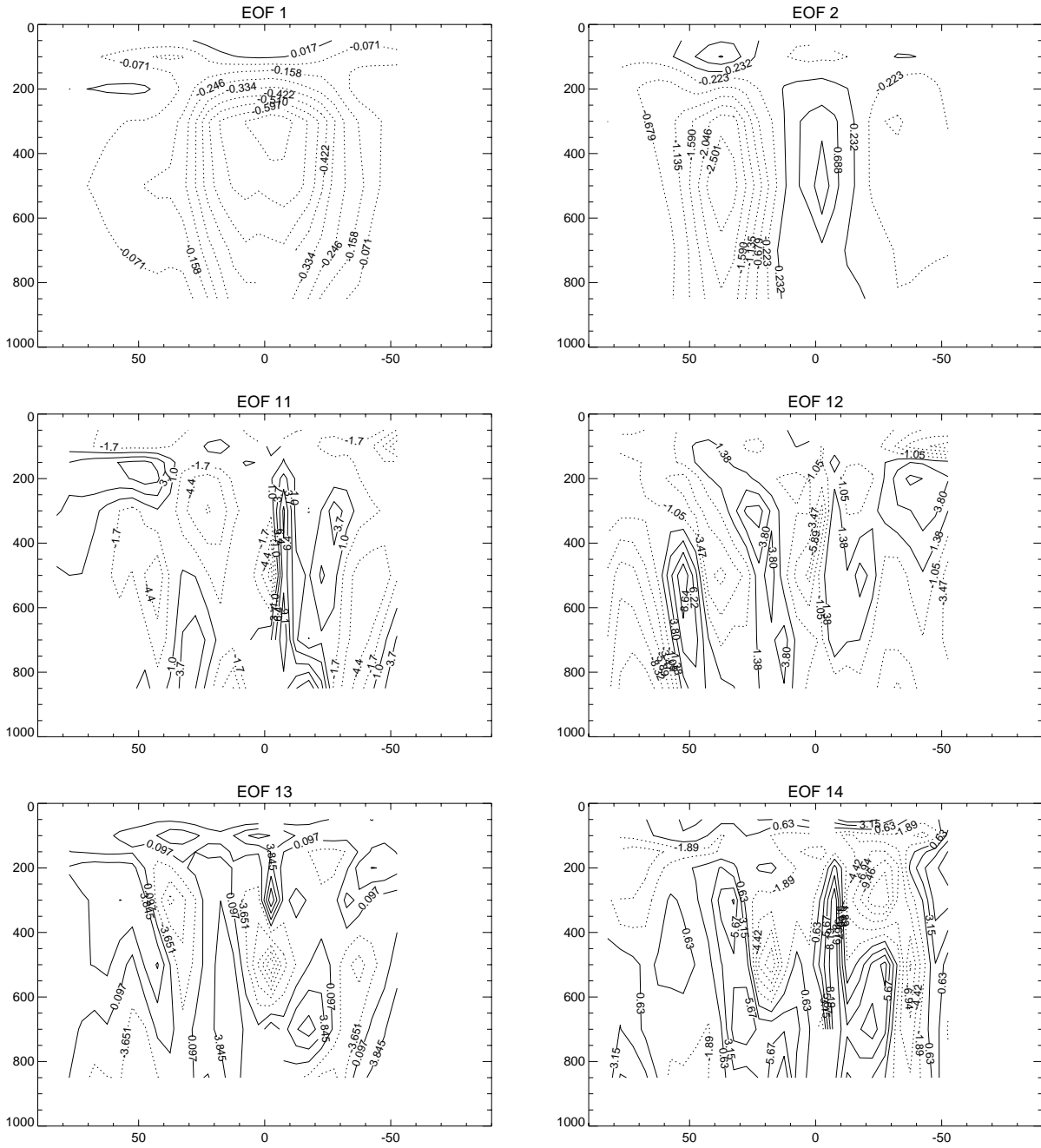
Fig. 9. EOFs 1-2 and 11-14 as estimated from the HadCM2 control run. Contour interval is chosen to be 1/10 the range of the values in each pattern.
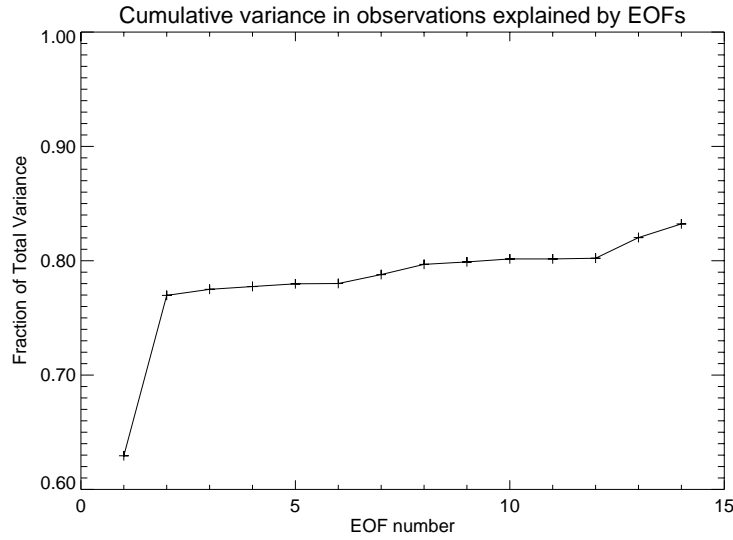
**Fig. 10.** Cumulative variance explained by EOF decomposition of observations.
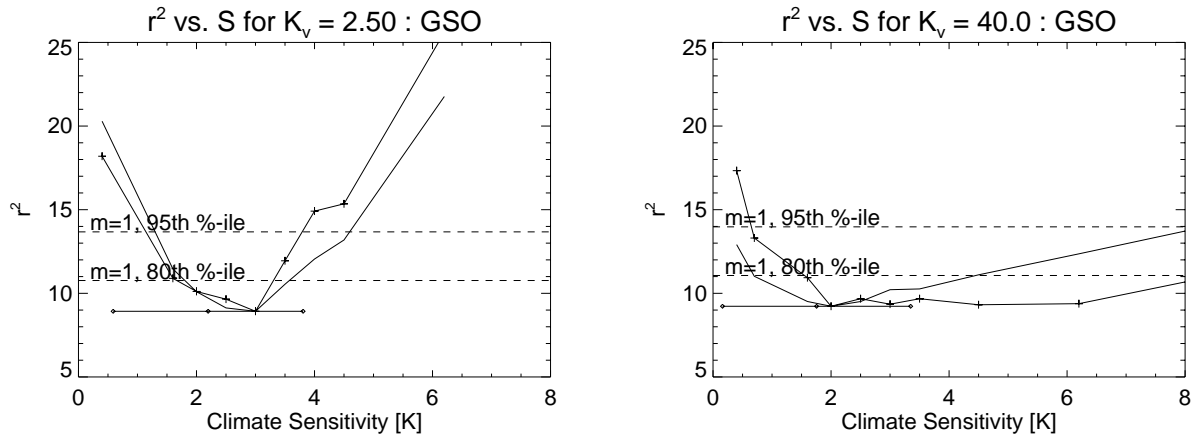
Fig. 11. The dependency of r^2 on climate sensitivity for $K_v = 2.5$ and 40.0 cm^2/s for the model response to GSO forcing and compared against pseudo-observations (i.e. model response at minimum location). $+$ symbol designates comparison with observations and no symbol indicates comparison with model at location of minimum r^2 for comparisons to observation. The r^2 values from the "perfect model" case are inflated such that the minimum value matches that from the fit with observations.
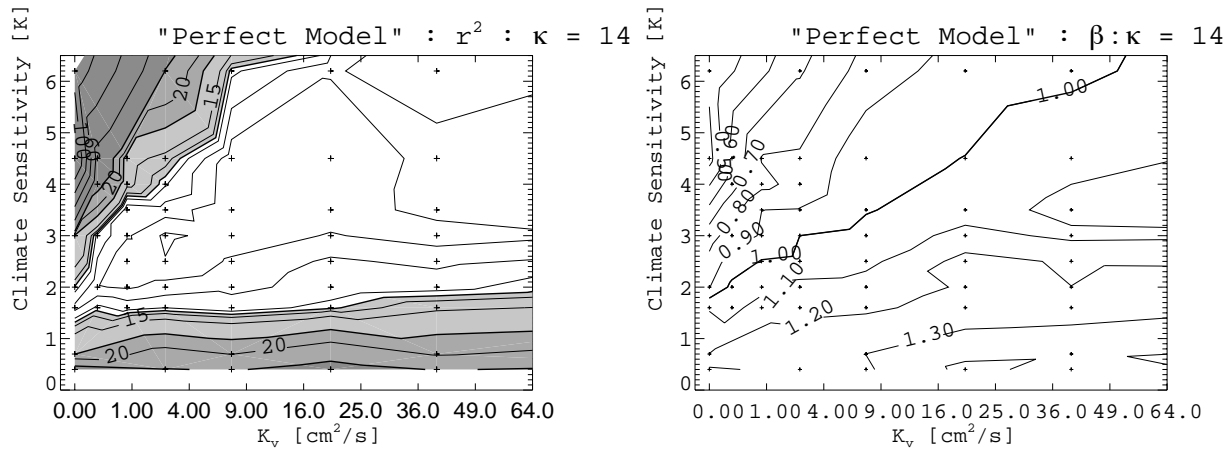
Fig. 12. The dependency of r^2 and β on both climate sensitivity and K_v for the model response to GSO forcing and compared against pseudo-observations (i.e. model response at minimum location determined from the fit to observations). To compare with Figure 13, the values of r^2 have been inflated such that the minimum value matches that from the fit with observations.
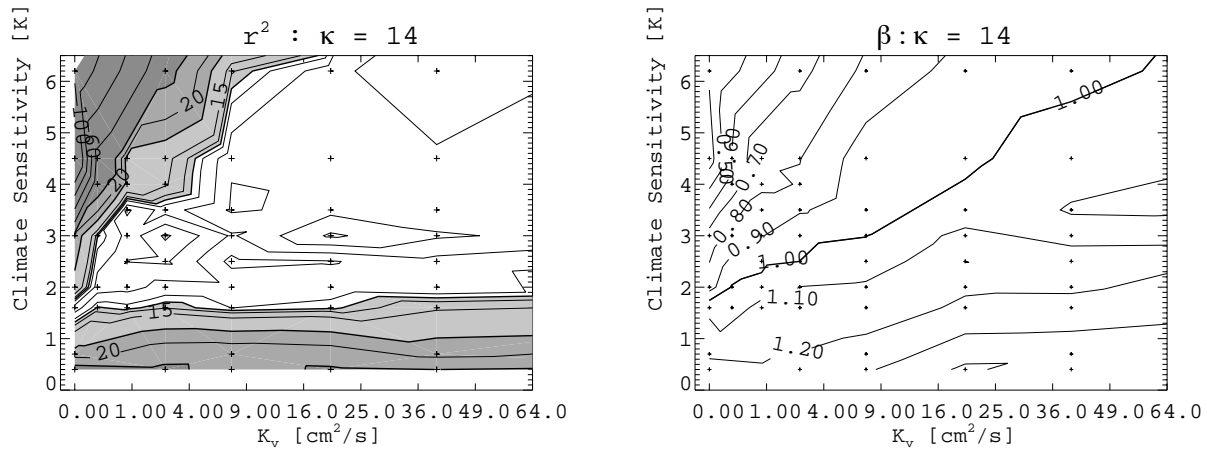

Fig. 13. The dependency of r^2 and β on both climate sensitivity and K_v for the model response to GSO forcing and compared against observations. (See text for explanation of shaded regions.)
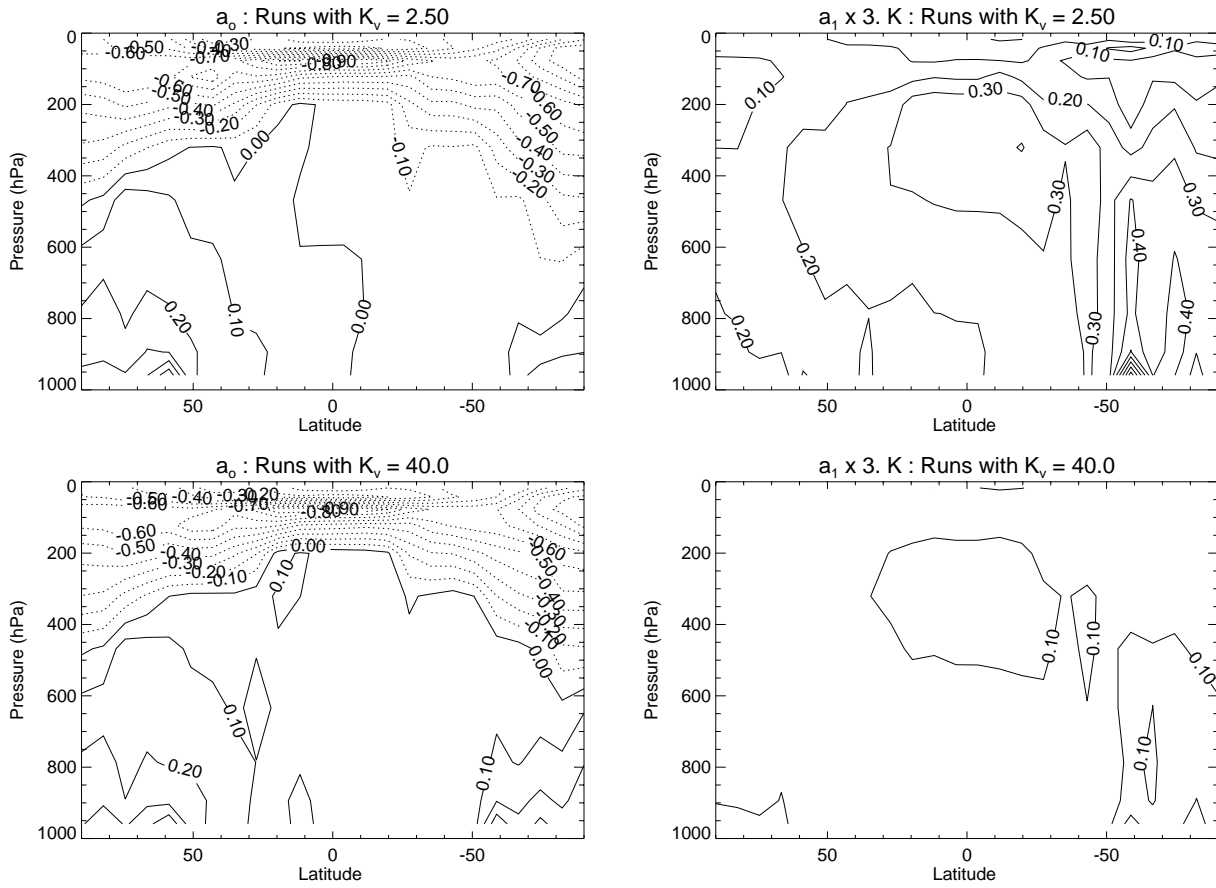
Fig. 14. The distribution of parameters, a_0 and a_1, for the linear regression model, $T_{i,j} = a_0 + a_1 S$, where $T_{i,j}$ is the temperature change at a given latitude-height location and K_v is held fixed. To compare a_0 and a_1, we have multiplied a_1 by the typical range of S to indicate the degree to which the trend term will alter the pattern of temperature change.
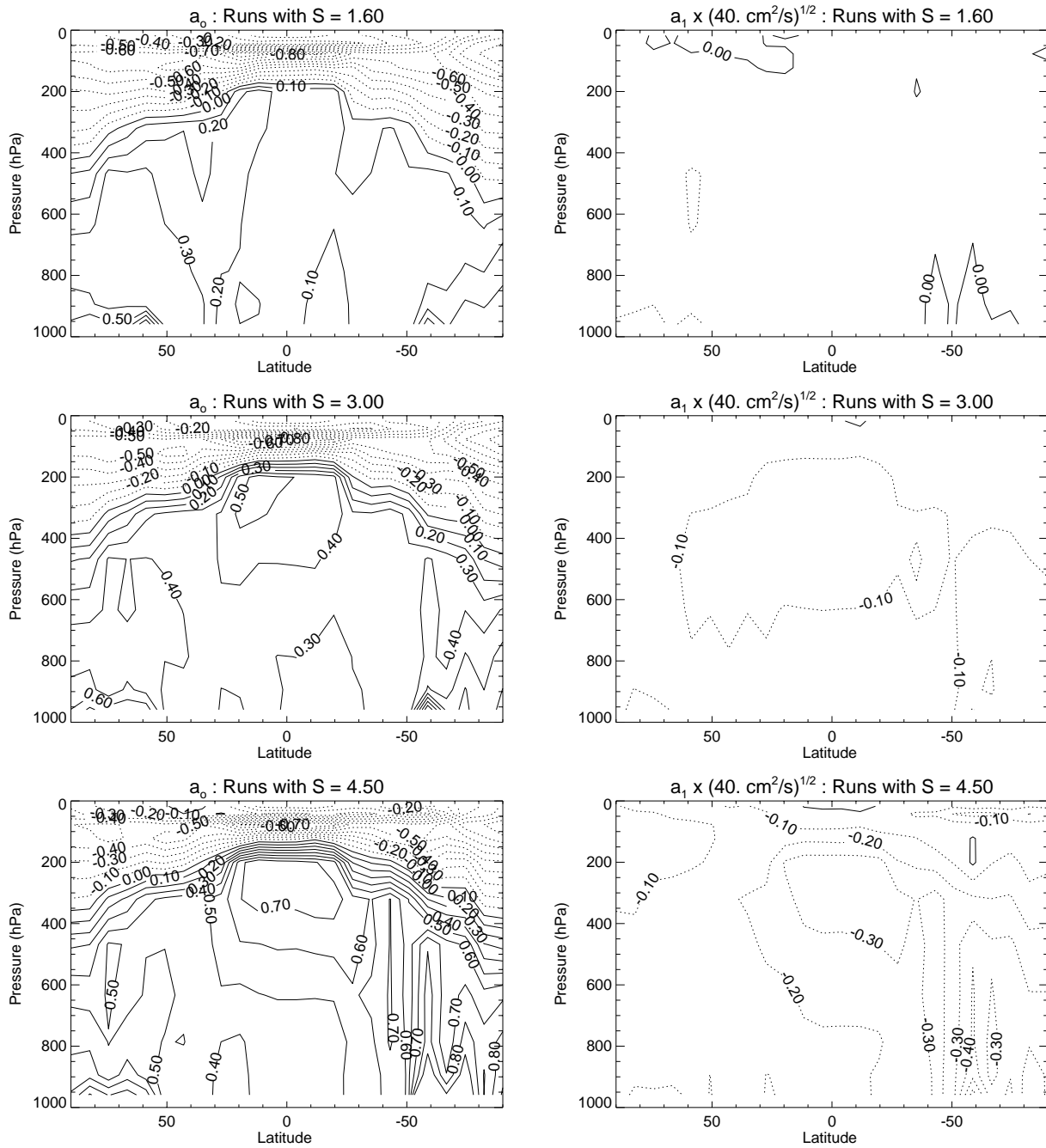
Fig. 15. Same as in Figure 14 except that the linear regression model is $T_{i,j} = a_0 + a_1 K_v^{1/2}$ and climate sensitivity is held fixed. In this case, a_1 is multiplied by $\sqrt{40 cm^2/s}$.
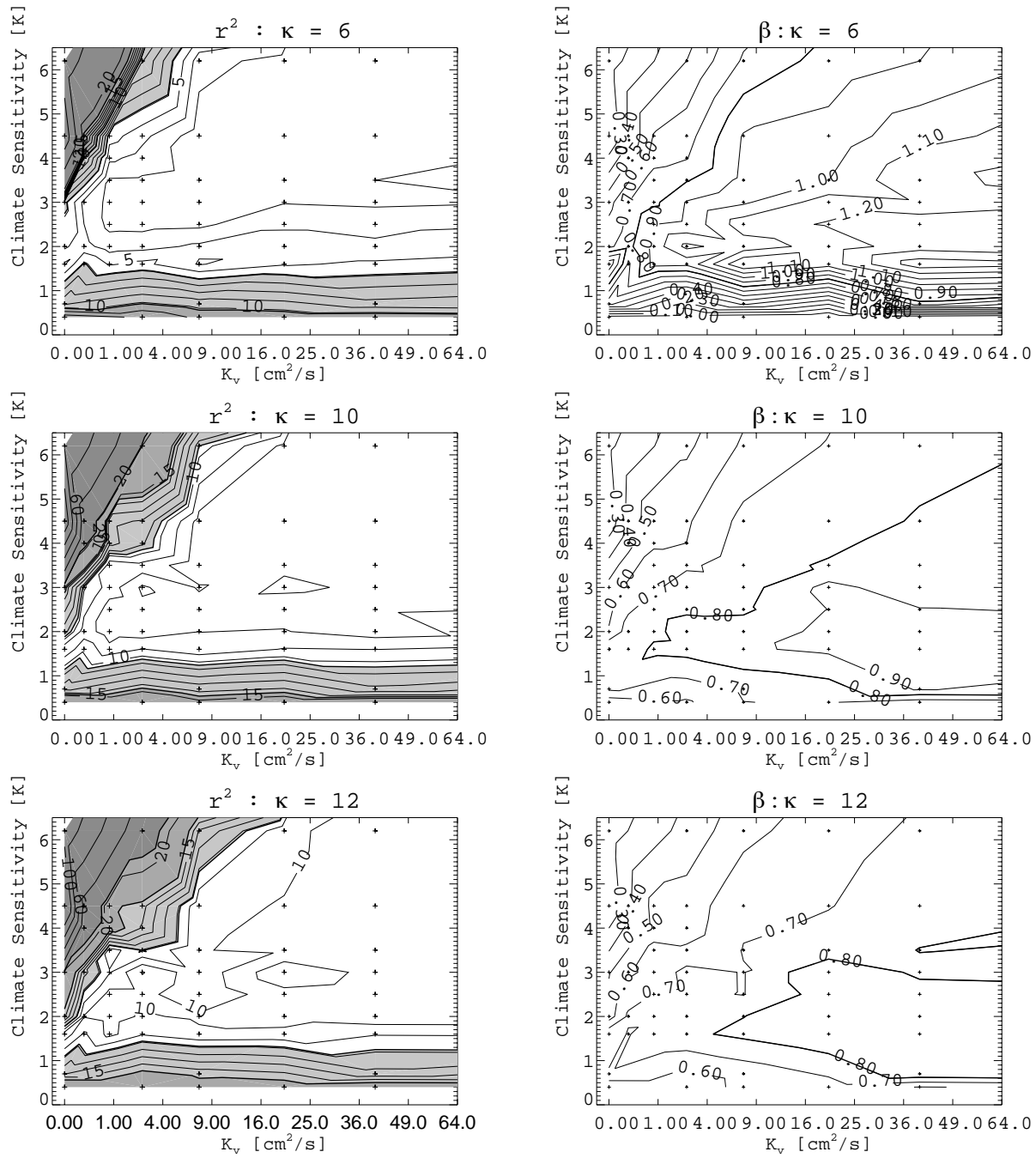
Fig. 16. The dependency of the distribution of r^2 and $\tilde{\beta}$ on κ. The $\tilde{\beta} = 0.8$ contour is thickened to illustrate its movement.